Structure and Reactivity of Binuclear Cu Active Sites in Cu-CHA Zeolites for Stoichiometric Partial Methane Oxidation to Methanol

Laura N. Wilcox¹, Jose Rebolledo-Oyarce², Andrew D. Mikes¹, Yujia Wang³, William F. Schneider^{2,3*}, and Rajamani Gounder^{1,*}

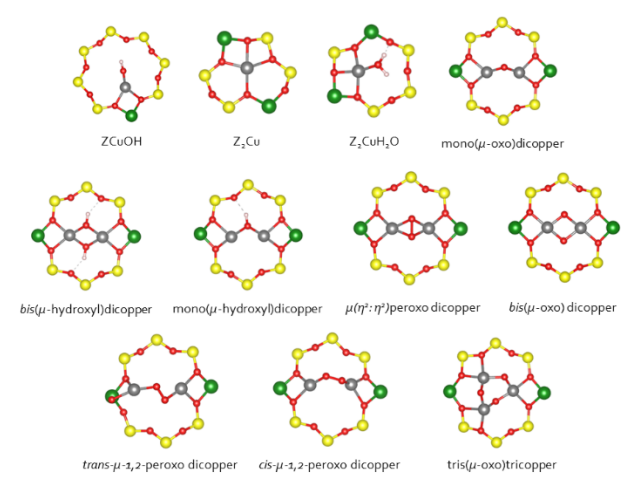
¹Charles D. Davidson School of Chemical Engineering, Purdue University, West Lafayette, IN, USA 47907 ²Department of Chemical and Biomolecular Engineering, University of Notre Dame, Notre Dame, Indiana, USA 46556

KEYWORDS: Binuclear active sites, Cu-zeolites, Partial methane oxidation, Spectroscopy, Titration

ABSTRACT: Aluminosilicate zeolites exchanged with copper ions facilitate partial methane oxidation (PMO) to methanol in stoichiometric oxidation and reduction cycles, yet the identities of active Cu sites and details of the reaction mechanism remain debated. Here, we use the high symmetry chabazite (CHA) zeolite framework as a model support to probe the relationship between bulk composition, Cu speciation, and response to various oxidizing and reducing treatments. Density functional theory and first-principles thermodynamics combined with statistical models reveal that Cu speciation and composition depend strongly on Al configuration and external gas conditions. Cu-CHA samples were synthesized to survey broad regions of Si/Al and Cu/Al composition space and framework Al proximity. Characterization by in situ X-ray absorption and UV-visible spectroscopy during exposure to different oxidation conditions reveal that the extent of Cu oxidation is sensitive to activation conditions and thus that both kinetic and thermodynamic factors influence Cu oxidizability in a given material. Similar characterizations during CO reduction reveals that CO titrates Cu²⁺ in amounts suggesting the presence of both O- and O₂-bridged species. In contrast, CH₄ and auto-reduction (He) treatments reduce similar but smaller numbers of Cu sites than CO, implicating O₂bridged Cu dimers as a potential common intermediate in the former reduction pathways. A systematic increase in methanol yields (per Cu) in stoichiometric PMO cycles increase with the fraction of binuclear O_x-bridged Cu sites suggests these species as active sites, as depicted in an updated PMO reaction mechanism.

1. Introduction

Cu-exchanged zeolites facilitate partial methane oxidation (PMO) to methanol in stoichiometric $^{1-4}$ and continuous $^{5-8}$ cycles. After high-temperature oxidative treatments (typically with O_2), a variety of Cu structures have been proposed to form on zeolite supports, including mononuclear sites (Cu $^{2+}$, [CuOH] $^+$), 9,10 binuclear sites (bis(μ -oxo)dicopper ([Cu(O)2Cu] $^{2+}$), 11,12 mono(μ -oxo)dicopper ([CuOCu] $^{2+}$), $^{1,13-17}$ μ -(η^2 : η^2)peroxo dicopper ([CuOCu] $^{2+}$), 1,15,16 bis(μ -hydroxyl)dicopper ([Cu(OH)2Cu] $^{2+}$), $^{19-21}$ trinuclear sites (mono(μ -oxo)tricopper), 3,22,23 and even higher nuclearity sites (Scheme 1). $^{24-26}$



Scheme 1. Schematic representations of Cu active site motifs proposed to form on Cu-exchanged zeolites after oxidation treatments. "Z" represents an Al-substituted Si site. Green: Al, yellow: Si, red: O, gray: Cu, pink: H.

Initial reports from Groothaert et al. identified bis(u-oxo)dicopper on O₂-activated Cu-MFI from UV-Visible spectra, an assignment supported with in situ extended X-ray absorption fine structure (EXAFS) and electron paramagnetic resonance (EPR) spectra. ^{11,12} Solomon and coworkers reported that mono-(μ-oxo)dicopper forms upon O₂ activation of Cu-MFI, ¹³ Cu-MOR, ²⁷ and Cu-CHA¹⁷ based on comparisons of resonance Raman spectra and density functional theory (DFT)-predicted structures of [Cu₂O]²⁺ cores sited within 8- and 10-membered rings (8-MR and 10-MR). Pappas et al. inferred that O_2 activation produces mono(μ -oxo)dicopper and trans- μ -1,2-peroxo dicopper from in situ X-ray absorption (XAS) and resonance Raman spectra of Cu-MOR²⁸ and Cu-CHA¹ zeolites of varying Cu and Al content, while Deplano et al.²⁹ and Pankin et al.³⁰ have used wavelet transform analysis of EXAFS spectra to identify mono(\(\mu\)-oxo)dicopper species on CHA and MOR. Ipek et al. identified a mono(μ -oxo)dicopper located in an 8-MR, a $[Cu_2O_2]^{2+}$ site bridging an 8-MR and a 6-MR, and a μ - $(\eta^2:\eta^2)$ peroxo dicopper site anchored on one silanol defect in the 8-

³Department of Chemistry and Biochemistry, University of Notre Dame, Notre Dame, IN 46556

MR as having the lowest free energies of formation at ambient temperatures, based on supercell DFT calculations. 15 Raman spectra of Cu-CHA were consistent with the presence of these three sites, while the mono- $(\mu$ -oxo)dicopper feature disappeared while that of the trans-μ-1,2-peroxo dicopper site persisted during longer O₂ activation times at ambient temperature, suggesting the existence of a pathway from a less stable former to more stable latter form. 15 Brezicki et al. concluded that mono- $(\mu$ -oxo)dicopper sites were responsible for selective methane oxidation to methanol while trans- μ -1,2-peroxo dicopper sites led to over-oxidation products (CO, CO₂) on Cu-MFI and Cu-MOR, based on evidence from UV-Visible spectra, reaction stoichiometries consistent with the total oxygen content among products formed (per active Cu), and DFT calculations of the relative stabilities of various binuclear Cu sites in MOR.¹⁶ Tsuchimura and co-workers studied Cu-CHA of varying Cu/Al ratio, observed mononuclear and various binuclear species in UV-visible spectra, and concluded that a mono(μ -oxo)dicopper species present at intermediate Cu loadings had the highest rates for catalytic methane oxidation.8 Lercher and coworkers reported evidence for tris(u-oxo)tricopper sites in Cu-MFI²³ and Cu-MOR^{3,22} based on CH₃OH yields (per Cu) that correlated linearly with one-third of the total Cu content, supported with in situ EX-

The number, structure, and reactivity of distinct $[Cu_xO_v]^{n+}$ site types on Cu-zeolite materials evidently depend on the framework topology, composition (Si/Al, Cu/Al), spatial arrangement of Al and Cu sites,³¹ and the specific oxidation treatments¹ and pre-treatment conditions³² used. Further, spectroscopic characterization and quantification present various challenges. Electronic paramagnetic resonance (EPR) potentially provides insight to Cu²⁺ speciation,³³ but interpretation is complicated by the EPR silence of Cu⁺ and some Cu²⁺ due to antiferromagnetic coupling.³⁴ Further, EPR is unable to directly access conditions of catalyst activation and reduction treatments of relevance for PMO. The use of UV-visible spectroscopy to interrogate the fate of binuclear Cu structures is challenged by overlapping d-d transition features and the heterogeneity of any given sample, which leads to an unknown ensemble of Cu sites and finite-temperature (thermally-induced) dynamics and restructuring that broadens all transitions.31 Thus, it is perhaps unsurprising that various $[Cu_xO_y]^{n+}$ site motifs have been proposed to facilitate PMO, given the large variation in zeolite topologies studied (e.g., MFI, MOR, CHA, AEI, MAZ) and reaction protocols used (e.g. O₂ activation time, temperature, and pressure),³² which influence the active Cu sites formed according to in situ Raman spectroscopy¹⁵ and methanol yields quantified by stoichiometric PMO.¹ In particular, the influence of framework Al arrangement within a given zeolite has been studied less extensively than the influences of zeolite topology or bulk composition, but this material property strongly influences extraframework metal speciation. Li et al. used supercell DFT models to compare free energies of Fe_xO_yH_zⁿ⁺ species as a function of Al location in CHA to show that Fe²⁺ exchange at a 6-MR is energetically favorable and produces a site $(\alpha$ -Fe)³⁵ with favorable energetics for PMO after N₂O activation.³⁶ Consistent with these predictions, Dusselier and coworkers synthesized Fe-CHA with different framework Al arrangements to demonstrate that 6-MR Al site pairs (i.e., second- or third-nearest neighbor) stabilize the dominant active site for stoichiometric PMO.³⁷

Experimental spectroscopic and titrimetric data and DFT calculations in CHA show that Cu²⁺ ions preferentially exchange into the same 6-MR paired Al site ("Z₂Cu"), while [CuOH]⁺ complexes exchange at a single framework Al in a 8-MR ("ZCuOH").³⁸ Thus, even for the simplest case of mononuclear Cu²⁺ ion sites exchanged onto the CHA framework, which contains a single crystallographically-unique lattice tetrahedral site (T-site), different populations of Cu site types are present among CHA samples of similar composition but different framework Al arrangements resulting from the specific crystallization methods used.^{39–42} Prior work showed

that Cu-CHA samples synthesized to emphasize different framework Al arrangements and thus extraframework Cu^{2+} site types, interrogated by *in situ* spectroscopy, stoichiometric PMO studies, and theoretical calculations, revealed differences in the kinetics of dioxygen activation and assigned both mono- $(\mu$ -oxo)dicopper and *trans-\mu*-1,2-peroxo dicopper as PMO active sites. ⁴³ Additionally, *trans-\mu*-1,2-peroxo dicopper sites were proposed to undergo O–O bond scission to form mono- $(\mu$ -oxo)dicopper sites, via incompletely understood mechanisms, with increasing time in dry O₂ treatment ¹⁵ that can be accelerated with the addition of H₂O. ⁴³

On a given Cu-zeolite, the formation of binuclear O_x-bridged Cu sites depends on various material properties including the Cu speciation, density, and proximity. Li et al. used in situ UV-Visible spectroscopy experiments corroborated by DFT models to show that ZCuOH-containing Cu-CHA zeolites form binuclear Oxbridged Cu species after high temperature O₂ treatment (723 K) that subsequently reduce in CO (523 K), while Z₂Cu-containing CHA zeolites remain unchanged after either O₂ or CO treatments.³¹ van Bokhoven et al. used X-ray diffraction (XRD), DFT, and XAS to examine the formation of PMO active sites in Cu-MOR and Cu-MAZ, proposing that proximal [CuOH]⁺ species^{19,25,44} and adjacent [CuOH]⁺ and Cu²⁺ sites can form O_x-bridged Cu species.⁴⁵ DFT has been used to probe dicopper structures and reactivity in zeolites; 17,20,46-48 yet, models commonly assume the locations of lattice Al T-sites, 49 thus missing the heterogeneity in Cu structure and reactivity introduced by lattice Al distributions. Early DFT calculations demonstrated the sensitivity of the geometric and electronic structures of $[Cu_2O_x]^{2+}$ cores to the location and orientation of Al T-sites. ^{50–53} Li et al. ³¹ and Bregante et al. ⁴³ found spectral features sensitive both to dicopper structure and Al siting. Göltl et al. used first-principles thermodynamics to compare the stability of $[Cu_2O_xH_y]^{n+}$ species as a function of Al location, proposing hydroxylated dimers as PMO intermediates.²⁰ Xie and co-workers used DFT models and CO and H2 TPR to conclude that the MFI framework stabilizes various forms of mono- $(\mu$ -oxo)dicopper sites.⁵⁴ The literature thus supports a prominent role of framework Al arrangement on the structure and reactivity of Cu species in zeolites for PMO reactions.

Here, we combine experiments and DFT-based models to interrogate this sensitivity across a set of compositions and reaction conditions. A suite of Cu-CHA zeolites was prepared with varying distributions of two-Al exchangeable (nominally Z₂Cu) and one-Al exchangeable (nominally ZCuOH) sites.³⁸ These samples were evaluated for the stoichiometric PMO reaction, and Cu structures were characterized using in situ X-ray absorption and UV-Visible spectra after exposure to different reducing environments (CO, CH₄, inert) and stoichiometric PMO reaction steps. First principles thermodynamic models are used to determine the relationship between Al proximity, Cu speciation, and stability at activation conditions, and statistical models used to predict the fractions of Cu site motifs as a function of Cu and Al content at those conditions. Experiment and theory support the formation of distinct binuclear O/O₂-bridged Cu species with distinct PMO reactivity, and an updated proposal of the elementary steps involved in stoichiometric PMO reaction cycles on Cu-zeolites.

2. Experimental Methods

2.1. Zeolite Synthesis and Aqueous Ion Exchange

CHA zeolites were synthesized with varying bulk Al content (Si/Al = 4.5–25) and varying fractions of 6-MR paired Al sites (i.e., 2 Al in a 6-MR in 2NN or 3NN configurations) according to methods reported previously that involve hydrothermal crystallization using different structure directing agents (SDA) or Al reagents,³⁹ or interzeolite conversion (FAU to CHA) routes,^{37,55} CHA was synthesized with precursors including Na⁺ as the inorganic SDA, N,N,N-trimethyl-1-adamantylammonium (TMAda⁺) as the organic

SDA, and various Al (e.g., aluminum hydroxide, aluminum isopropoxide, FAU zeolite) and Si (e.g., colloidal silica, sodium silicate) sources. CHA zeolites containing predominantly 6-MR isolated Al configurations (i.e., 1 Al in a 6-MR) were synthesized using solely TMAda⁺ as the SDA.³⁹

After the desired crystallization time, solids were recovered and washed with alternating steps of deionized (DI) water (18.2 MΩ) and acetone (99.9 wt%, Sigma Aldrich) using 70 cm³ solvent per g solids. The washing and centrifugation process was repeated until the pH of the supernatant was constant between washes. The final wash step was completed with water to remove any residual acetone. Solids were recovered from centrifugation and dried overnight in stagnant air at 373 K. Dried solids were then treated in flowing dry air (zero grade, Indiana Oxygen; 1.67 cm³ s⁻¹) at 853 K (0.0167 K s⁻¹) for 10 h to remove organic material. Following this treatment, XRD patterns (Fig. S1, SI) and micropore volumes estimated from Ar adsorption isotherms (87 K, Fig. S2, SI) gave results consistent with the CHA framework topology.

H-form zeolite samples were obtained after aqueous-phase ammonium nitrate (99%, Sigma Aldrich, 1 M NH₄NO₃, 150 g solution per g zeolite) exchange at ambient temperature for 24 h, followed by washing and centrifugation in DI water (70 cm³ per g solids) five times. Solids were dried overnight in stagnant air at 373 K and then treated in flowing dry air (zero grade, Indiana Oxygen; 1.67 cm³ s⁻¹) at 773 K (0.0167 K s⁻¹) for 4 h to remove NH₃.

Aqueous NH₄⁺ ion-exchange (1M NH₄NO₃, 24 h) followed by NH₃ temperature programmed desorption (TPD) was used to quantify the number of Brønsted acid sites on each sample (Table S1, SI). The number of 6-MR paired Al sites was measured by Co²⁺ titration using protocols described in our prior reports,³⁹ validated by measuring Co²⁺ ion-exchange isotherms to verify saturation of all 6-MR paired Al sites, UV-Visible spectra of Co-zeolites that did not show the presence of Co_xO_y species, and residual H⁺ sites on Co-zeolites by NH₃ titration that yielded a site balance consistent with the replacement of two H⁺ sites per Co²⁺ ion.

Cu-form zeolites were obtained by aqueous ion-exchange of H-zeolites with an aqueous copper nitrate solution (98%, Alfa Aesar, 0.001-0.2 M Cu(NO₃)₂, 150 g solution per g zeolite), while controlling the pH of the solution to ~4 by dropwise addition of 0.1 M ammonium hydroxide (28-30% NH₃ basis, Sigma Aldrich). The solution was stirred for 4 h at ambient temperature, and solids were recovered by centrifugation and washed five times with DI water (70 cm³ per g solids). After drying overnight in stagnant air at 373 K, samples were treated in 1.67 cm³ s⁻¹ of air flow (zero grade, Indiana Oxygen) at 773 K (0.0167 K s⁻¹) for 4 h.

2.2. Characterization Methods

2.2.1. Elemental Analysis

Atomic absorbance spectroscopy (AAS) with a PerkinElmer AAnalyst 300 Atomic Absorption Spectrometer was used to determine elemental compositions of Al, Na, and Cu on samples. Al was measured in a reducing acetylene/nitrous oxide flame at the wavelength 309.3 nm. Na and Cu were measured at the wavelengths 589.0 nm and 324.8 nm, respectively, in an oxidizing air/acetylene flame. Samples were prepared by dissolving approximately 0.020 mg of zeolite in 2 g of hydrofluoric acid (48 wt%, Sigma Aldrich), followed by a dilution with 50 g of deionized water (18.2 M Ω). Known standard solutions of each element were measured to create a calibration curve to then calculate elemental compositions for the samples. Si/Al ratios were determined using the Al weight fraction together with the unit cell formula for chabazite.

2.2.2. Diffuse Reflectance UV-Visible Spectroscopy

Diffuse reflectance UV-visible spectra were recorded using a Varian Cary 5000 UV-Vis-NIR Spectrophotometer attached with a Praying Mantis diffuse reflectance accessory. Baseline spectra

were recorded using PTFE (polytetrafluoroethylene with 200 μ m particle size, Sigma Aldrich), BaSO₄ (barium sulfate, Sigma Aldrich), or the parent H-CHA as a 100% reflectance reference material. Cu-CHA (sieved to 180–250 μ m aggregates) was held in dry air (commercial grade, Indiana Oxygen; 5.6 cm³ s⁻¹ g⁻¹) while increasing the temperature from ambient to 673–773 K (0.167 K s⁻¹) for 1–6 h. Samples were then cooled to 473 K under air flow, and then further to 300 K. Spectra were collected during the cooling period from 473 K to ambient temperature.

After exposure to high temperature air (673–773 K, up to 6 h), samples were reduced with 5 kPa CO in balance He (99.999% UHP, Indiana Oxygen; 5.6 cm 3 s $^{-1}$ g $^{-1}$) at 523 K (0.5 K s $^{-1}$), until spectra stopped changing. Then, samples were flushed with inert He (99.999% UHP, Indiana Oxygen) at 523 K for 0.5 h to remove physisorbed CO, and further cooled to 300 K in He.

Following the same oxidation treatment above, samples was exposed to inert environment (99.999% UHP He, Indiana Oxygen; 5.6 cm³ s⁻¹ g⁻¹; purified using an oxygen moisture trap (Matheson, MTRP-0019-XX)) while the temperature was increased from ambient to 723 K (0.167 K s⁻¹) for 2 h. Samples were cooled to ambient temperature prior to collecting spectra.

Prior to methane introduction, samples were first exposed to air (21 kPa O_2) and the temperature was increased from ambient to 723 K (0.167 K s⁻¹) for 6 h. Samples were then cooled to ambient temperature, and then flushed in He to remove residual O_2 . Next, the gas flow was switched to CH₄ (4.9 kPa balance He, 99.999% UHP, Indiana Oxygen) and the temperature was increased from ambient to 473 K (0.167 K s⁻¹) for 0.5 h. Spectra were collected after cooling to ambient temperature. UV-Vis spectra in Kubelka-Munk units are shown in the main text, and spectra in reflectance (%R) are shown in the Supporting Information (Section S3, SI).

2.2.3. X-ray Absorption Spectroscopy

X-ray absorption spectroscopy experiments were performed at the Advanced Photon Source (APS), Argonne National Laboratory in Lemont, Illinois, in sector 10 Materials Research Collaborative Access Team (MR-CAT). The insertion device beamline at sector 10 (10-ID) and the bending magnet beamline at sector 10 (10-BM) were used for *in situ* experiments. A Cu metal foil reference spectrum (edge energy of 8979 eV) was measured simultaneously with each sample spectrum collected to calibrate the X-ray beam for spectral measurements at the Cu K-edge. All X-ray absorption near edge structure (XANES) spectra were analyzed in WinXAS and normalized using first and third order polynomials for background subtraction of the pre- and post-edges, respectively. XANES spectra were analyzed using multivariate curve resolution-alternating least squares (MCR-ALS) analysis, following the methods of Kvande et al.⁵⁶ and Martini et al.⁵⁷, as described in detail in Section S6 (SI).

Several oxidation and reduction treatments were studied on Cu-CHA samples at 10-ID. Auto-reduction in He (UHP, 99.999%) through an oxygen moisture trap (Matheson, MTRP-0019-XX) was studied at 648 K and 723 K until spectra stopped changing (up to 2 h). Oxygen activation (21 kPa O₂, balance He) was also monitored between 648-723 K and holding for up to 2 h. Methane (4.1 kPa CH₄, balance He), was introduced to samples at 473 K until spectra stopped changing (0.25–2 h). Then, a vapor stream of 2.5 kPa H₂O (N₂ carrier gas through a water saturator) at 473 K until spectra appeared as rehydrated as Cu²⁺ (typically 0.5 h).

A "six-shooter" reactor was used to house 5 different Cu-CHA samples that were pelletized and treated simultaneously during each oxidation and CO reduction treatment at 10-BM. The samples were dehydrated in O₂ (10.1 kPa in balance He, UHP, Praxair) at 723 K (0.167 K s⁻¹) for 1 h. Following the oxidation treatment, CO (1 kPa, balance He) was introduced to the sample at 523 K. Spectra were collected until XANES spectra remained unchanged, taken to be the point of completion of the CO reduction treatment.

2.3. Stoichiometric PMO Reactions

Cu-zeolites were activated in air (16 cm³ s⁻¹ g⁻¹) at 723 K (0.167 K s⁻¹) for 6 h, then cooled to ambient temperature in He (99.999% UHP, Indiana Oxygen; 16 cm³ s⁻¹ g⁻¹). Methane (20 kPa CH₄, balance UHP He, 9.6 cm³ s⁻¹ g⁻¹) was introduced and heated to 473 K (0.167 K s⁻¹) and held for 0.5 h following the protocol of Alayon et al.⁵⁸ Prior to water extraction, the apparatus was purged with He (UHP, Indiana Oxygen, 9.6 cm³ s⁻¹ g⁻¹) for 0.167 h. Next, water was introduced via a flowing wet He stream (2.5 kPa H₂O; 9.6 cm³ s⁻¹ g⁻¹) at 473 K for 1 h. An online Agilent 5973N mass selective detector (MSD) was used to quantify methanol (m/z = 31) using argon (99.999% UHP, Indiana Oxygen) as a calibration standard (m/z = 40) by introducing pulses of argon of known quantities using the reactor bypass after completion of the reaction procedure, and to monitor CH₄ (m/z = 16), H₂O (m/z = 18), CO (m/z = 28), CO₂ (m/z = 44), CH₂O (m/z = 29), and C₂H₆O (m/z = 45).

2.4. Computational Methods

2.4.1. DFT Calculations

Calculations were performed using the Vienna Ab-initio Simulation Package (VASP)⁵⁹ version 5.4.1. Periodic spin-polarized DFT calculations were performed with the Perdew, Burke, and Ernzerhof (PBE) exchange-correlation functional on a CHA supercell containing 36 T-sites, using previously reported lattice constants.³⁶ The projected augmented wave (PAW) method^{60,61} was used to describe the core-electron interactions, and a plane-wave basis set was included to a kinetic cutoff energy of 400 eV. Bands were sampled at the Γ point. Self-consistent-field energies were converged to 10⁻⁶ eV and structures relaxed until all forces were less than 0.03 eV/Å. Semiempirical D3 dispersion correction with Becke-Johnson damping^{62,63} does not have a significant impact on the determination of the most thermodynamically stable species (as shown in Fig. S31, SI). Harmonic vibrational frequencies were calculated by finite differences on atomic forces. Atomic displacements were 0.01 Å and restricted to Cu atoms and bridging ligands, leaving zeolite atoms fixed. These vibrational frequencies were used to compute zero-point vibrational energies (ZPE) and entropy difference between Cu species. All imaginary and low (<100 cm⁻¹) frequencies were set to 100 cm⁻¹. All structures can be found in CONTCAR format as Supporting Information.

2.4.2. Ab Initio Free Energies

To compare the thermodynamic stability of mononuclear and binuclear Cu sites as a function of Al site configurations and external conditions, formation (free) energies were calculated with respect to Z_*Cu , H_2O (g), and O_2 (g). With these references, the mononuclear Cu site formation reaction is written as:

$$Z_*Cu + \frac{x}{2} \left(H_2O - \frac{1}{2}O_2 \right) + \frac{y}{2}O_2 \rightarrow Z_*CuH_xO_y$$
 (1)

To establish the connection between an isolated Al site and a paired Al site, the Cu exchange energy was calculated between the two sites, following the protocol defined by Paolucci et al.³⁸:

$$ZCuOH + Z_2H_2 \rightarrow Z_2CuH_2O + ZH$$
 (2)

The binuclear Cu site formation reaction is written as:

$$ZCu/ZCu + \left(\frac{x}{2}\right)H_2O + \left(\frac{2y - x}{4}\right)O_2 \rightarrow Z_2Cu_2H_xO_y$$
 (3)

and the energy to place two ZCu species in the same supercell was calculated using the following reaction:

$$2ZCu + Z_2H_2 \rightarrow ZCu/ZCu + 2ZH \tag{4}$$

Here, Z indicates an anionic Al framework site, ZH an isolated Brønsted site, and Z₂H₂ one of various realizations of two proximal Al, and ZCu/ZCu the energy of two proximal Cu at the same Al pair site. Supercells comprising 36 T-sites are constructed to assure

atom conservation. To include the conditions of activation, we write the formation free energy as:

$$\Delta G_{a,b,c,d}(T, P_{H_2O}, P_{O_2})$$

$$= \Delta E_{a,b,c,d} - T\Delta S^{\circ,ST}(T) + \nu_{O_2} \Delta \mu_{O_2}(T, P_{O_2}) + \nu_{H_2O} \Delta \mu_{H_2O}(T, P_{H_2O})$$
(5)

$$\Delta\mu_i = \left(G^{\circ}(T) - G^{\circ}(T = 0 K)\right) + RT \ln\left(\frac{P_i}{P^{\circ}}\right) \tag{6}$$

where $\Delta E_{\mathrm{a,b,c,d}}$ is the DFT-computed reaction energy and $\Delta S^{\mathrm{o,ST}}$ the reaction entropy. For the latter, we use a model previously shown to provide a good approximation to the entropy difference between a free and adsorbate-covered site, which treats adsorbed species as retaining 2/3 of their gas-phase translational entropy as captured in the Sackur-Tetrode equation⁶⁴:

$$\Delta S^{\circ,ST}(T) = \left(S_{Z_*Cu_W}A(T) - S_{Z_**Cu_W}(T) \right)$$

$$\approx \frac{2}{3} k_B \ln \left[\left(\frac{2\pi M_{x,y} k_B T}{h^3} \right)^{\frac{3}{2}} \left(\frac{k_B T}{P^{\circ}} \right) \frac{e^{5/2}}{N_A} \right]$$
(7)

where $M_{x,y}$ is the total mass of the adsorbed species and P^0 is the standard pressure, 1 bar. Finally, v_i and $\Delta \mu_i$ are the stoichiometric coefficient and the chemical potential differences of H₂O and O₂ gases between 0 K and the conditions of interest, which was calculated using the ideal gas-approximation. To compare, we calculated the formation free energy using Harmonic Approximation (HA) for the entropy term (detailed in Section S32, SI).

3. Results and Discussion

3.1. Compositional Characterization of Cu-CHA Zeolites After High-Temperature O₂-Activation

Cu-CHA samples of varying Al (Si/Al = 4.5-25) and Cu (Cu/Al = 0.08-0.44) content were synthesized as described in our prior work³⁸ to contain varying amounts of 2Al and 1Al sites, which nominally exchange Z₂Cu and ZCuOH, respectively; salient characterization data are summarized in Table 1 (additional data in Section S1, SI). Samples are given a unique letter code and denoted as Cu-CHA(X)-Y-Z, where X and Y are respectively the Si/Al and Cu/Al ratios, and Z is the nominal number density of ZCuOH sites per cha cage. The number of Co²⁺-titratable sites was used as a proxy for the number of Z₂Cu sites, with the remainder Cu accounted as ZCuOH (details in Section S2, SI). To capture the tendency of some nominally ZCuOH to form binuclear Cu sites upon O₂ activation, we turn to DFT calculations and statistical models. We consider many possible Al-Al pairs in the CHA lattice and the binuclear Cu structures they may host. We searched for mono(µoxo)dicopper, $bis(\mu$ -oxo)dicopper, μ - $(\eta^2:\eta^2)$ peroxo dicopper, trans-\u03c4-1,2-peroxo dicopper, cis-\u03c4-1,2-peroxo dicopper, mono(\u03c4hydroxyl)dicopper, and $bis(\mu$ -hydroxyl)dicopper structures (Scheme 1) over Al-Al pairs ranging from 2NN in a 6-MR up to 4NN location in an 8-MR (relaxed structures, raw energies, vibrational spectra of all species in Sections S8-S9, SI). We computed formation energies of these binuclear Cu structures using ZCu, H₂O and O2 as energy references; using ZCu as a Cu reference allows us to relate binuclear Cu structures to their reduced form, Cu⁺.

Results are reported in Figure 1a as a function of Al-Al separation. A water-coordinated mononuclear Cu^{2+} site, Z_2CuH_2O , is lowest in formation energy at all Al-Al separations, because this structure benefits from interactions of both Cu and protons with anionic framework oxygen. $Bis(\mu$ -hydroxyl)dicopper is the lowest energy binuclear Cu structure at all Al-Al separations, with monoand dioxygen-bridged species higher in energy. Formation energies of a given binuclear Cu site, and the identity of the lowest energy structure, depend strongly on Al-Al separation. Such sensitivity to Al-Al separation is consistent with the DFT results of Wang et al. 65

Table 1. Structural and site characterization of Cu-CHA samples.

Sample ^a	ID	Si/Al ^b	Cu/Al ^b	Cu (per unit cell) ^c	Cu (per cage) ^d	Z ₂ Cu (per cage) ^e	ZCuOH (per cage) ^e
Cu-CHA(25)-0.37-0.15	A	25	0.37	0.53	0.18	0.03	0.15
Cu-CHA(4.5)-0.08-0	В	4.5	0.08	0.64	0.21	0.21	0
Cu-CHA(4.5)-0.21-0	С	4.5	0.21	1.68	0.56	0.56	0
Cu-CHA(15)-0.09-0.07	D	15.6	0.09	0.22	0.07	0	0.07
Cu-CHA(15)-0.11-0.09	Е	15.6	0.11	0.26	0.09	0	0.09
Cu-CHA(15)-0.24-0.19	F	15.5	0.24	0.58	0.19	0	0.19
Cu-CHA(15)-0.44-0.35	G	14.3	0.44	1.06	0.35	0	0.35
Cu-CHA(21.6)-0.06-0.05	Н	21.6	0.06	0.14	0.05	0	0.05
Cu-CHA(15)-0.04-0.03	I	15.2	0.04	0.10	0.03	0	0.03
Cu-CHA(13)-0.10-0.09	J	12.9	0.10	0.28	0.09	0	0.09
Cu-CHA(15)-0.07-0.05	K	15.5	0.07	0.16	0.05	0	0.05
Cu-CHA(15)-0.05-0.04	L	15.2	0.05	0.13	0.04	0	0.04
Cu-CHA(15)-0.07-0.05	M	14.7	0.07	0.16	0.05	0	0.05

^a Sample nomenclature is Cu-CHA(X)-Y-Z. X = Si/Al, Y = Cu/Al, Z = ZCuOH/cage.

To inform the conditions that prevail during zeolite activation, we translated DFT formation energies to free energies at 723 K and 21% partial pressure of O_2 and 0.01% partial pressure of H_2O , at 1 bar total pressure, with results shown in Figure 1b. A Cu^{2+} ion exchanged at a 3NN or 2NN 6-MR Al pair site is lowest in free energy at these conditions. O-bridged dicopper sites compete with and become more stable than isolated Cu^{2+} with increasing Al-Al separation, with mono(μ -oxo)dicopper and mono(μ -hydroxyl)dicopper species similar in free energy. O_2 -bridged dicopper sites lie higher in free energy than O-bridged sites, a prediction that will be sensitive to both the DFT and free energy models used.

Regardless, calculations predict 6-MR Al-Al pairs to preferentially populate with Z_2 Cu before 8-MR Al-Al pairs are populated with dicopper structures. As shown in Figure 1b, mono(μ -oxo)dicopper and mono(μ -hydroxyl)dicopper species have similar free energy, which might rationalize why both hydroxyl-bridged^{7,20} and mono(μ -oxo)-bridged^{17,48,65} dicopper sites have been reported in Cu-CHA, suggesting a pool of binuclear Cu structures that are present in some experimental Cu-CHA materials, dependent on synthesis conditions and Cu and Al loading. The sensitivity of site composition to Al-Al pair site highlights the role of zeolite topology in influencing Cu speciation, helping to rationalize, for instance, the observation that larger average distances between Al pairs in a framework influences speciation between PMO-active and inactive species. $^{19,66-70}$

Next, we used these free energy results to predict equilibrium composition phase diagrams as a function of Si/Al, Cu/Al, and framework Al siting. First, Al are distributed randomly on a large 2,304 T-site CHA supercell to the target Si/Al value, enforcing Löwenstein's rule, creating a distribution consistent with that observed and expected to hold in CHA samples synthesized with Na⁺ and thus having 6-MR Al-Al pair sites. ^{39,41,42} As motivated by Figure 1b, the sites are then titrated to the target Cu/Al ratio, first populating 6-MR Al-Al pair sites as Z₂Cu, then remaining 4NN and 3NN 8-MR Al-Al pair sites as binuclear Cu structures, and finally assigning any remaining Cu as ZCuOH (details in Section S12, SI).

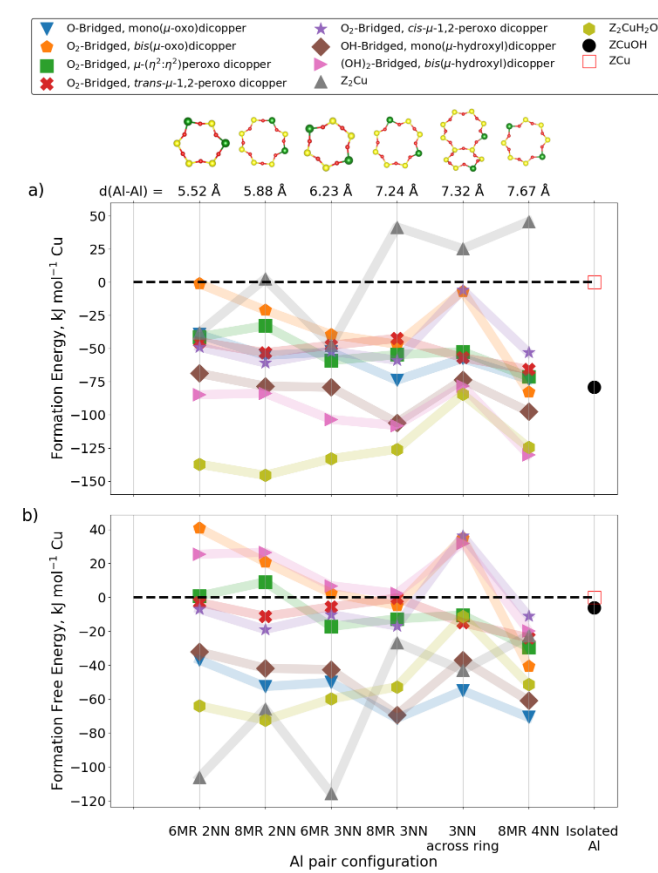


Figure 1. (a) DFT-computed formation energies of mononuclear and binuclear Cu sites as a function of Al-Al separation, referenced to isolated ZCu, O₂ and H₂O, and (b) corresponding free energies of formation at 723 K, 21% O₂, and 0.01% H₂O at 1 bar total pressure (activation conditions). Green: Al, yellow: Si, red: O.

^b Al content was determined by AAS and Si content was determined from unit cell of CHA calculations. Uncertainty is ±10%.

^c Calculated by multiplying Cu/Al by the number of Al per 36 T-site unit cell.

^d Calculated using Eq. (3) from Section S2, SI.

^e Calculated from Co²⁺ titration and Cu siting models reported previously (details in Section S2, SI).²⁸

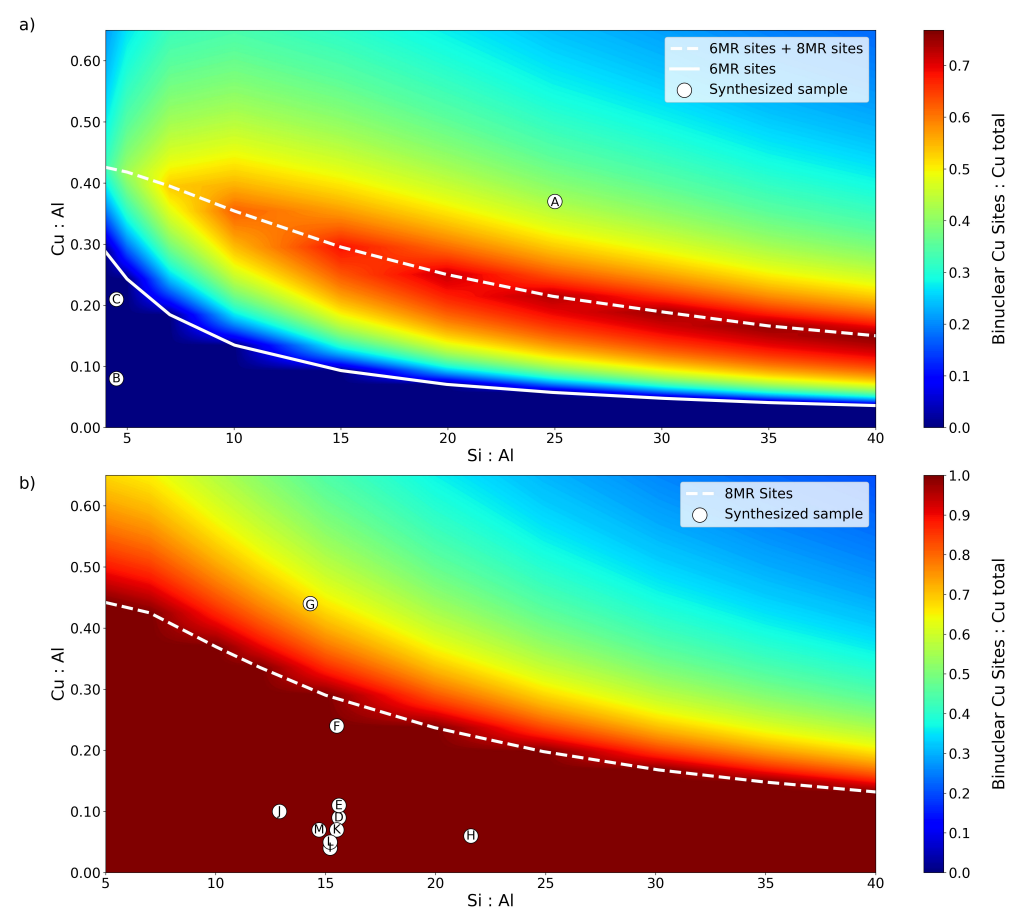


Figure 2. Predicted equilibrium composition phase diagrams at activation conditions (723 K, 21% O₂, 0.01% H₂O, 1 bar total pressure) as a function of Si/Al and Cu/Al. Solid white lines and dashed white lines indicate Z₂Cu and binuclear Cu saturation, respectively, and color indicates fractional binuclear Cu population. (a) Al atoms distributed randomly obeying Löwenstein's rule, consistent with Na⁺-prepared samples. (b) Al atoms distributed randomly obeying Löwenstein's rule and preventing 6-MR Al pairs, consistent with Na⁺-free syntheses. White circles with letters correspond to experimental samples in Table 1.

Results are shown as the composition phase diagram in Figure 2a. The solid line indicates the expected saturation of Z_2Cu sites³⁸ and the dashed line indicates the subsequent saturation of dicopper sites. The color scale indicates the fraction of total Cu expected to be present as binuclear species, a quantity that increases towards the latter saturation line before decreasing; it never reaches unity. Further indicated are the first three samples from Table 1 (Samples A-C). Sample A is expected to have a mixture of Z_2Cu , a significant quantity of binuclear species, and isolated ZCuOH species, while samples B and C contain only Z_2Cu species, consistent with predictions based on Co^{2+} titration results.

To capture the Al distribution expected to prevail in CHA samples synthesized (with TMAda⁺ only) to contain primarily isolated Al, we performed the same simulations while forbidding occupancy of two Al in the same 6-MR.^{39,42} Results are shown in Figure 2b. In contrast to Figure 2a, these materials are expected to be dominated by binuclear Cu species over a large composition range, including all samples from Table 1 that do not exchange Co²⁺ (Samples D-M) and samples that do (but only at higher Cu/Al ratios; Sample A). Wijerathne et al.⁶⁶ conducted an extensive exploration of the competition between Cu monomers and dimers in various Al pair configurations across different zeolite frameworks. Their estimated phase diagrams resemble those presented in Fig. 2. However, they suggested that in zones with a rich fraction of Cu dimers (as shown in Fig. 2b), a small fraction of two proximal

ZCuOH could coexist. The predictions of Figure 2 assume thermodynamics alone govern Cu speciation; yet, the mechanisms of forming binuclear Cu structures upon reaction with O_2 are not fully known. Mono(μ -oxo)dicopper sites can form upon condensation of two proximal ZCuOH sites that liberate water: 1,4,15,38

$$2[CuOH]^+ \rightarrow [Cu - O - Cu]^{2+} + H_2O$$
 (8)

or from the condensation of a Z₂Cu site and a proximal ZCuOH site to form a dicopper and Brønsted acid site:

$$[Cu]^{2+} + [CuOH]^{+} \rightarrow [Cu - O - Cu]^{2+} + [H]^{+}$$
 (9)

Dioxygen-bridged sites can plausibly form through oxidation of two proximal ZCu sites:

$$2[Cu]^{+} + O_2 \rightarrow [Cu - O_2 - Cu]^{2+}$$
 (10)

An alternative path to dioxygen-bridged sites, proposed based on DFT calculations on Cu-MFI, involves disproportionation of two ZCuOH sites into Cu(I) and Cu(III)O⁺, followed by the combination of two proximal CuO⁺ species to form Cu-O₂-Cu⁷¹:

$$2[CuOH]^+ \rightarrow Cu(I) + [CuO]^+ + H_2O$$
 (11)

$$[CuO]^+ + [CuO]^+ \rightarrow [Cu - O_2 - Cu]^{2+}$$
 (12)

Experimental evidence to detect and identify a Cu(III)O⁺ intermediate is lacking, however, and previously computed phase

diagrams for Cu-CHA zeolites with 1 Al site do not predict ZCu(III)O to exist under relevant O_2 activation conditions (i.e., 723 K, 21 kPa O_2). ³⁸ Given that the barriers for these site formation reactions are likely sensitive to Cu-Cu and Al-Al pair separations, it is expected that the distributions of Cu sites obtained on a Cu-zeolite material after high temperature O_2 activation treatment may deviate from the equilibrium predictions of Fig. 2.

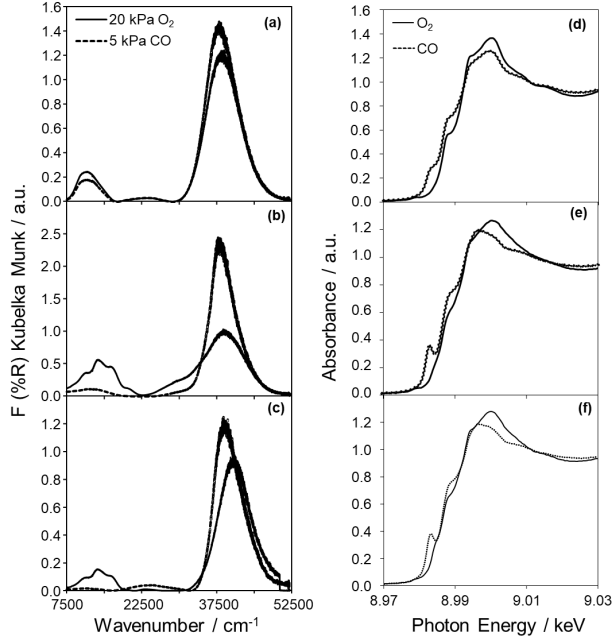


Figure 3. (a-c) UV-Visible spectra collected after treatment in 20 kPa O₂ at 723 K (solid line) followed by reduction in 5 kPa CO at 523 K (dashed line) and (d-f) *in situ* XANES after oxidation treatment (20 kPa O₂, 723 K, 1 h) shown in black followed by reduction in CO (1 kPa CO, 523 K) shown as dashed. Spectra shown for (a/d) Sample C, (b/e) Sample A, (c) Sample F, and (f) Sample D.

UV-Visible spectra of Samples A, C, and F (Table 1) after a high-temperature O₂ treatment (21 kPa O₂, 723 K, 2 h) are shown in Figure 3; each spectrum contains d-d transition features for Cu²⁺

ions (~8,000-16,000 cm⁻¹) and a ligand-to-metal charge transfer (LMCT) band (~30,000-50,000 cm⁻¹), consistent with prior reports. 16,31,72,73 UV-Visible spectra of samples A and F (Fig. 3b and c) also exhibit low-energy LMCT bands (~24,000–30,000 cm⁻¹) indicative of multinuclear Cu species, ^{11–15,17,73–76} consistent with the composition predictions in Figures 2a (sample A) and 2b (sample F). Precise O_x-bridged Cu structures cannot be determined by UV-Vis, as shown by time dependent-DFT (TD-DFT) simulations of UV-Vis spectra that predict d-d and LMCT transitions of similar energies for various O-/O2-bridged binuclear Cu sites at distinct 8-MR 2 Al arrangements in CHA (Fig. S3, SI). 21,31 Raman spectra show both mono- $(\mu$ -oxo) and O₂-bridged structures are present on these Cu-CHA samples after high-temperature O2 treatments (Fig. S6, SI).43 Thus, while Figure 2b predicts all Cu to be present as mono- $(\mu$ -oxo) at equilibrium based on the thermodynamic predictions of Fig 1b, kinetic factors likely result in the formation of a mixture of binuclear Cu structures.

In situ XAS was used to monitor the Cu oxidation state in samples A, C, and D following a high-temperature O2 treatment (20 kPa O₂, 723 K, 1 h), with the Cu²⁺/Cu⁺ distribution quantified by MCR-ALS analysis of the XANES region reported in Table 2 (spectra and reconstructions shown in Figs. S15-S26, SI). Sample C is expected to contain only Z₂Cu sites based on its synthesis and composition (Table 1) and phase diagrams (Fig. 2a), but is predicted by MCR-ALS fitting to contain 15% Cu⁺ (Table 2), as a result of overestimation of the Cu⁺ from MCR-ALS (discussion in Section S6, SI). Thus, we estimate a ±0.15 uncertainty in Cu⁺ fractions quantified from MCR-ALS fitting. Sample D is expected to contain a larger density of ZCuOH sites than sample C (Table 1), all of which are predicted to form binuclear Cu²⁺ structures after O₂ activation (Fig. 2b), consistent with XANES (Table 2). Residual Cu⁺ (34%) may reflect some nominally pairable Cu sites that for unknown kinetic reasons, are not oxidized by O2, in addition to overestimation of the Cu⁺ fraction from MCR-ALS fitting. Sample A is expected to contain an even larger density of ZCuOH sites (than samples D and C, Table 1) and predicted to contain a mixture of Z₂Cu, binuclear Cu, and ZCuOH sites (Fig. 2b). XANES spectra show 47% Cu(I), attributable to both the overestimation of Cu⁺ from MCR-ALS and that ZCuOH and ZCu sites are similar in free energy at this condition (Fig. 1b); thus, any ZCuOH sites that persist after O₂ activation may appear in a reduced Cu⁺ state.

Table 2. Cu(I) and Cu(II) fraction on Cu-CHA samples after different treatments, determined from MCR-ALS fitting of in situ Cu K-edge XANES spectra.

suu Cu K-euge AANES spectia.												
Sample	ID	O ₂ Activation (21 kPa O ₂ , 723 K) ^a		Auto-reduction (101.3 kPa He, 723 K) ^a		CH ₄ reduction (4.1 kPa CH ₄ , 473 K) ^a		CO reduction (1 kPa CO, 523 K) ^a				
										Cu(I)	Cu(II)	Cu(I)
		Cu-CHA(4.5)-0.21-0	C	0.15	0.85	0.17	0.83	0.37	0.63	0.59	0.41	
Cu-CHA(15)-0.09-0.07	D	0.34	0.66	0.75	0.25	0.86	0.14	0.95	0.05			
Cu-CHA(25)-0.37-0.15	A	0.47	0.53	0.87	0.13	0.92	0.08	0.89	0.11			

^a Uncertainty in fitted values is ± 0.15 .

3.2. Quantification of Binuclear Cu Sites by UV-Visible and XAS Spectroscopy after CO Reduction

We next interrogated high-temperature O₂-activated Cu-CHA samples by CO reduction, which is expected to oxidize to CO₂ upon reaction with O atoms of extraframework Cu complexes.^{53,77} As a control, a Cu-CHA sample containing solely Z₂Cu sites (sample C, Fig. 2a) was exposed to high-temperature oxidation (20 kPa O₂, 723 K) and subsequent CO reduction (5 kPa CO, 523 K), and led to only minor changes in UV-Vis spectra (Fig. 3a); the small loss in d-d intensity may reflect the presence of a minority amount of residual CO-reducible (presumably binuclear) Cu sites. Sample A,

expected to contain a mixture of binuclear and mononuclear Cu sites showed the near complete disappearance of LMCT bands near $\sim 16,379,\,20,077,\,$ and $27,000\,$ cm $^{-1}$ (Fig. 3b) indicative of multinuclear O_x -bridged $Cu,^{53}$ with residual d-d transitions reflecting Z_2Cu and spatially isolated ZCuOH sites that do not form O_x -bridged binuclear Cu species. Sample F, expected to contain only binuclear Cu structures (Fig. 2b), showed the complete disappearance of LMCT bands (Fig. 3c) for multinuclear O_x -bridged Cu species. Sample F, expected to contain only binuclear Cu structures (Fig. 3c) for multinuclear O_x -bridged Cu species.

Analogous CO reduction treatments were performed while measuring *in situ* XAS spectra. For all samples, XANES spectra showed the appearance of Cu⁺ features after CO exposure (Fig. 3d-f). Again, as a control, sample C was exposed to these treatments

and showed a non-negligible amount of reduced Cu(I) (59%, Table 2, Fig. 3a,d). Sample A showed a higher amount of reduced Cu(I) (89%, Table 2, Fig. 3b,e), and sample D an even higher amount of reduced Cu(I) (95%, Table 2, Fig. 3f).

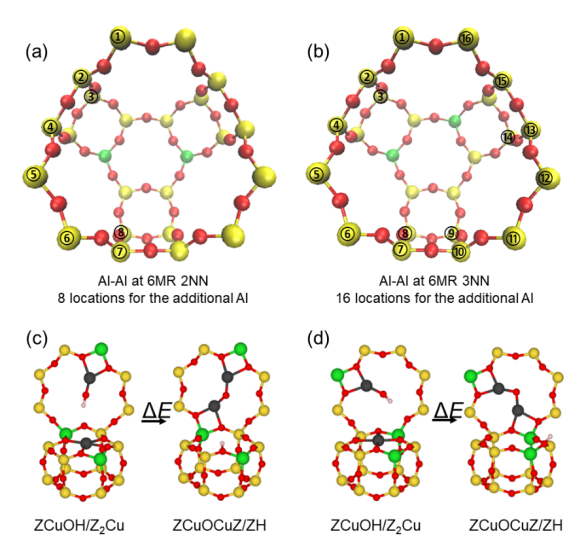


Figure 4. (a,b) Illustration of 24 3-Al combinations including a 6-MR Al pair and proximal 8-MR Al. (c,d) Representative structures before and after reorganization of a ZCuOH/ Z_2 Cu pair to a mono- $(\mu$ -oxo) Cu site. Green: Al, yellow: Si, red: O, gray: Cu, pink: H.

The qualitative changes in d-d transition band intensities in UV-Vis spectra (Fig. 3a-c) and quantitative changes in Cu⁺ fractions derived from XANES spectra (Fig. 3d-f, Table 2) after CO reduction are qualitatively consistent with the binuclear Cu site fractions predicted by Figure 2; however, the appearance of Cu(I) features in sample C highlight the presence of a small number of reducible Cu species that stands in contrast with other characterizations and the predictions of Figure 2. The speciation model underlying Figure 2a partitions all Al into isolated (1 Al) and paired site (2 Al) configurations, but higher-order proximal Al ensembles could alter that enumeration. To consider this possibility, we computed the energy for a three Al-containing ZCuOH/Z₂Cu ensemble to transform to a binuclear ZCuOCuZ site and Brønsted (ZH) site. We considered 24 different combinations of Z₂Cu sites and an additional ZCuOH in a proximal 8-MR, as shown in Figures 4a and 4b, with example reactions shown in Figures 4c and 4d and reaction energies in Figure 5. Nine binuclear mono- $(\mu$ -oxo) Cu sites combinations are preferred over the Z₂Cu form, consistent with an underestimation of binuclear sites in Figure 2a.

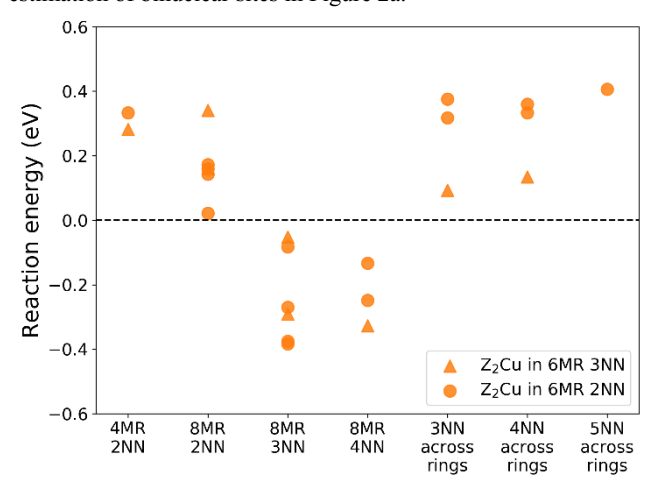


Figure 5. DFT-computed ZCuOH/Z₂Cu \rightarrow ZCuOCuZ/ZH reaction energies vs. mono-(μ -oxo) Cu dimer host site. Triangles and circles indicate Z₂Cu site type.

To estimate the frequency of these three Al configurations, we distributed Al onto a 972 T-site CHA supercell obeying Löwenstein's rule, from Si/Al = 3 to 40, and counted configurations; results are shown in Figure 6. The three Al sites are present at all Si/Al ratios and represent a significant fraction of the total Al sites at low Si/Al. The experimental observation that some Cu sites are reduced in CO in the sample predicted to contain only Z_2 Cu sites (Sample C, Fig. 2a) may thus result from binuclear Cu sites that are miscounted as Z_2 Cu in the analysis of Figure 2. Thus, we expect Fig. 2a to underpredict CO reducible sites, especially at low Si/Al. EPR, UV-Vis, photoluminescence and Fourier-transform infrared (FTIR) evidence obtained on Cu-MOR samples suggests a similar combination of Cu^{2+} ions adjacent $[CuOH]^+$ ions to participate in CH_4 oxidation.

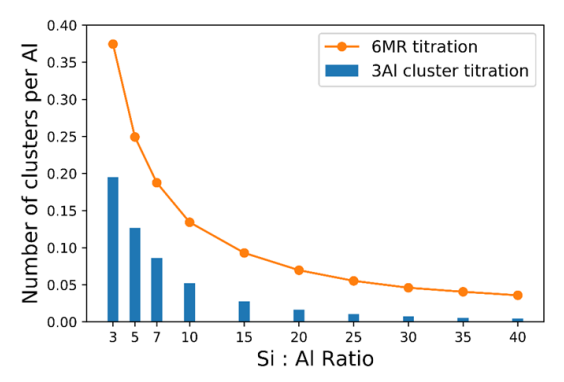


Figure 6. Predicted number of Al-Al-Al configurations at Si/Al = 3 to 40 under Löwenstein's rule in CHA. The number of 6MR Al-Al pairs under Löwenstein's rule at each Si/Al ratio is shown as reference (also reported in Figure 2a).

Next, we quantified the binuclear Cu sites present on Cu-CHA samples after a high-temperature oxidation treatment (21 kPa O₂, 723 K, 2 h) from the amount of CO₂ produced upon a subsequent reduction with CO in a temperature-programmed reduction (TPR) experiment (Table S2, SI). A plausible reaction pathway for CO reduction of mono-(μ -oxo)dicopper sites is:⁵³

$$CO + [Cu - O - Cu]^{2+} \rightarrow CO_2 + 2Cu^+$$
 (13)

An analogous reaction can be written for CO reduction of O_2 -bridged dicopper sites, with a stoichiometry of 1 equivalent of CO_2 produced per Cu:

$$2CO + [Cu - O_2 - Cu]^{2+} \rightarrow 2CO_2 + 2Cu^{+}$$
 (14)

Sample C, predicted to contain only Z₂Cu sites by the model in Figure 2a, produces 0.28 CO₂/Cu (Table S2, SI), consistent with XANES data (Table 2) and further supporting the prediction in Figure 6 that some binuclear Cu sites form even in this composition regime. Sample A, predicted to contain ~40% of Cu in binuclear structures according to Figure 2a, produces 0.27 CO₂/Cu, consistent with the binuclear state being predominantly mono(μ oxo)dicopper (if all sites were this structure, Eq. 13 predicts 0.20 CO₂/Cu) and some as O₂-bridged dicopper sites. Samples E and J are predicted to contain only binuclear Cu sites (Fig. 2b), and give CO₂/Cu > 0.5 (Table S2, SI), consistent with a mixture of O- and O₂-bridged dicopper sites. Given that CO reduces both O- and O₂bridged dicopper sites (Table S2, SI), the number of binuclear Cu sites varies non-monotonically with ZCuOH density (Figure S9, SI). Other samples expected from Figure 2b to have high fractions of binuclear Cu sites (including samples F, G, H, L), produce < 0.5 CO₂/Cu. Figure 2b thus overestimates the fraction of oxidized binuclear Cu sites in these samples, due to kinetic or mechanistic factors not captured in the thermodynamic prediction, as also evidenced in part by the non-zero fraction of Cu^+ after high-temperature O_2 treatment observed in such samples by XANES (Table 2). The precise composition of binuclear sites thus appears to be sensitive to local structure and pretreatment conditions and is influenced both by thermodynamic stability and kinetic accessibility.

3.3. Influence of ZCuOH Site Density on Auto-reduction Behavior

Cu²⁺ auto-reduction to Cu⁺ has been observed at high temperatures (> 650 K) in inert environments (e.g., He) on various Cuexchanged zeolites (e.g., MOR, MFI, CHA) by in situ XANES, and the evolution of O₂ during auto-reduction (700-1000 K) of Cu-MOR has been observed but not quantified by online mass spectrometry;67,78 yet, elementary step details and active site requirements for Cu²⁺ auto-reduction mechanisms remain unclear. Here, we studied the auto-reduction behavior (He, 723 K, up to 2 h) of three Cu-CHA zeolites of varying ZCuOH density (samples C and A of Fig. 2a and sample D of Fig. 2b) using in situ XANES, with spectra shown in Figure 7a-c and Cu(I) and Cu(II) fractions determined by MCR-ALS analysis of XANES spectra (Table 2). Cu²⁺ auto-reduction was relatively small on the Cu-CHA sample containing nominally only Z₂Cu sites (17% Cu(I), Sample C, Table 2), as observed previously. 1,46 On Sample D, which contains nominally only ZCuOH sites (Table 1) that are all predicted to form binuclear Cu structures (Fig. 2b), the auto-reduction treatment increased the Cu⁺ fraction from 34 to 75% Cu(I) (Table 2). On Sample A, which contains higher densities of ZCuOH sites than sample D (Table 1) that are expected to form a mixture of binuclear Cu structures and mononuclear Cu sites (Z₂Cu and ZCuOH) according to Figure 2b, the auto-reduction treatment increased the Cu⁺ fraction from 47 to 87% Cu+ (Table 2).

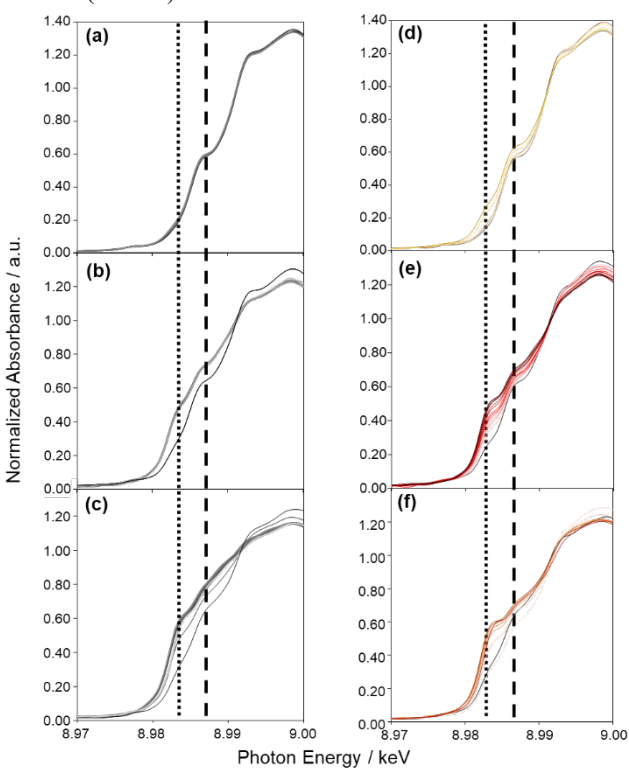


Figure 7. Transient (0–2 h) *in situ* Cu K-edge XANES collected on (a/d) Sample C, (b/e) Sample D, and (c/f) Sample A after respective treatments in auto-reducing (101 kPa He, 723 K) or CH₄-reducing environments (4.1 kPa CH₄, 473 K). The line (····) at 8.983 keV denotes Cu(I) and the line (---) at 8.897 keV denotes Cu(II). The oxidized state of each sample is shown in black, with Cu(I) increasing with additional exposure time in He or CH₄.

The fraction of auto-reducible Cu²⁺ sites increased with ZCuOH density among these samples, consistent with the hypothesis that two Cu species in close proximity (Eqs. 3 and 4) are required to form O/O₂-bridged binuclear Cu structures that can subsequently undergo auto-reduction:

$$Z_2Cu_2H_xO_y \rightarrow ZCu/ZCu + \left(\frac{x}{2}\right)H_2O + \left(\frac{2y-x}{4}\right)O_2$$
 (15)

On all the Cu-CHA samples studied, including those predicted in Figure 2b to contain only binuclear Cu suites, complete autoreduction to Cu⁺ was not observed. Furthermore, Figure 2 predicts a similar amount of binuclear Cu sites on samples A and D, yet a larger number of auto-reducible sites are observed on sample D, again suggesting that not all binuclear sites are auto-reducible.

The auto-reduction of binuclear Cu species was further monitored by in situ UV-Vis on sample A, chosen as a representative ZCuOH-containing sample (0.15 ZCuOH/cage), characterized to have 0.87 Cu(I)/Cu after auto-reduction treatments by in situ XANES (Table 2). Figure 8 shows UV-Vis spectra collected after treatment in O2 (21 kPa O2, 723 K) and then either exposure to an inert environment (He, 723 K) to initiate auto-reduction or to CO (5 kPa CO in He, 523 K). After O₂ activation, four distinct features in the d-d transition region (~8,000–16,000 cm⁻¹) and a feature in the low energy LMCT region (~24.000–30.000 cm⁻¹) are observed. Both auto-reduction and CO reduction led to partial disappearance of these bands, but to an apparently larger extent after CO reduction, suggesting that only a subset of binuclear Cu species that are reducible by CO are able to undergo auto-reduction. Given the greater extent of Cu²⁺ reduction after CO exposure observed with in situ XAS (Table 2), we conclude that CO reduces both O- and O2-bridged dicopper sites, according to Eqs. 13 and 14, respectively. We further propose that it is more likely that Cu-O₂-Cu species undergo auto-reduction, as also proposed by Brezicki et al., 16 given the elementary nature of eliminating molecular O2, in contrast to the non-elementary nature of Cu-O-Cu auto-reduction.

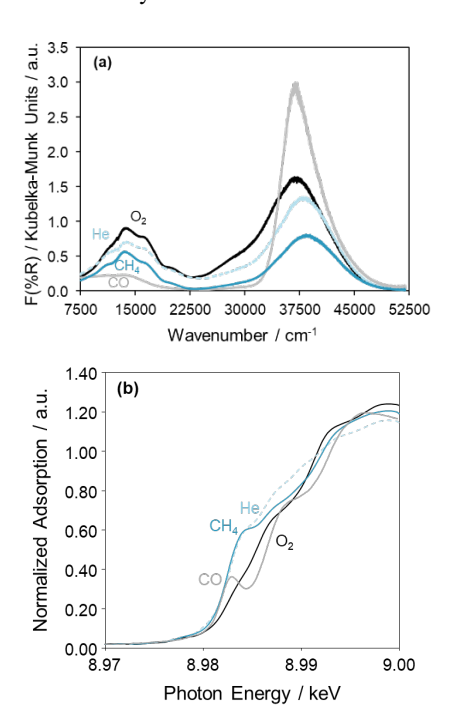


Figure 8. (a) UV-Visible spectra on Sample A after O₂ activation at 723 K in 20 kPa O₂ (black) followed either by the introduction of 101 kPa He at 723 K (--, light blue), or by the introduction of 4.1 kPa CH₄ at 473 K (blue) with a CO reduction treatment post-CH₄ treatment (light grey). 5 kPa CO reduction at 523 K is shown in

lightest grey to compare the reduction treatments. (b) In situ XAS spectra on Sample A after O_2 activation at 723 K in 10 kPa O_2 (black) followed either by the introduction of 101 kPa He at 723 K (--, light blue) or by the introduction of 4.1 kPa CH₄ at 473 K (blue), and a CO reduction treatment 1 kPa at 523 K (light grey).

The inability of all binuclear Cu structures to undergo autoreduction may reflect either an intrinsic thermodynamic or kinetic barrier to auto-reduction. Therefore, Eq. 15 was used to test the thermodynamic preference of various binuclear Cu structures to form Cu(I). 46,67,78 In Figure 9, we report the DFT-computed free energies of reaction (Eq. 15) as a function of Al-Al site proximity under the experimental auto-reduction conditions (723 K, 21×10⁻⁴ kPa of O₂, 0.01% of H₂O at 1 bar total pressure). First, an isolated ZCuOH site itself (at 1 Al site) is predicted to be at the boundary of stability against auto-reduction at these conditions (Fig. 9a, filled circle). Next, various binuclear Cu sites at 8-MR 3NN and 4NN Al-Al site pairs that are expected to dominate the species present experimentally are predicted to have varied resistance against autoreduction. Mono- $(\mu$ -oxo) and mono- $(\mu$ -hydroxyl) dimers are expected to be robust to auto-reduction at any Al-Al pair site, consistent with the DFT-predicted phase diagrams by Göltl et al., which report mono(μ -hydroxyl) dicopper to be most stable at autoreduction conditions.²⁰ In contrast, many O₂- and (OH)₂-bridged dimers are predicted to be slightly unstable (-40 kJ mol⁻¹) to slightly stable (20 kJ mol-1) against auto-reduction. Thus, the energetics of auto-reduction not only depends on Cu speciation but also on Al-Al pair location, where 8-MR 4NN and 3NN O-bridged dicopper sites have greater tendency to remain in their Cu(II) form, and thus would be unlikely to auto-reduce. Overall, these thermodynamic tendencies can rationalize the experimental observation that only a fraction of binuclear Cu sites auto-reduce (Table 2).

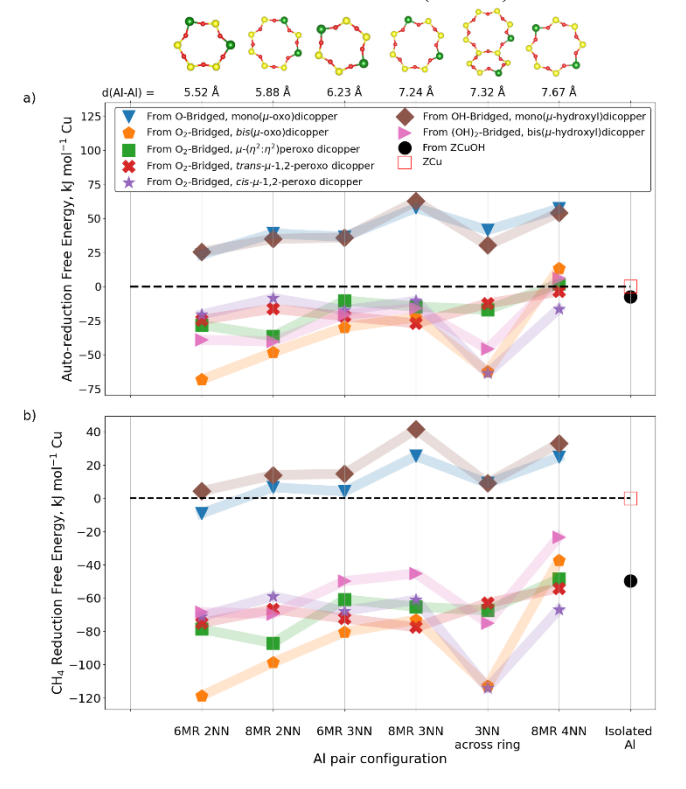


Figure 9. Reduction Free Energy: (a) auto-reduction free energy of various Cu structures (723 K, 21×10^{-4} kPa of O_2 , 0.01% of H_2O at 1 bar total pressure), and (b) CH₄ reduction free energies at various Cu(II) site types (473 K, 21×10^{-4} kPa of O_2 , 0.01% of H_2O , 4.1 kPa of CH₄, 1 bar total pressure).

In this auto-reduction environment, DFT suggests a slight thermodynamic tendency of isolated ZCuOH sites to auto-reduce to ZCu (Fig. 9a), but experimental XANES data show that not all ZCuOH sites can auto-reduce (Fig. 7, Table 2), suggesting a kinetic barrier to reduction. This would falsify one proposed auto-reduction mechanism¹ involving the reduction of a single ZCuOH site to ZCu while forming a hydroxyl radical (Eq. 16), which reacts with a second ZCuOH site to form water and [Cu(II)O]⁺ (Eq. 17):

$$[Cu(II)OH]^+ \leftrightarrow Cu(I) + OH \cdot \tag{16}$$

$$[Cu(II)OH]^{+} + OH \cdot \leftrightarrow [Cu(II)O]^{+} + H_{2}O$$
 (17)

resulting in the overall reaction:

$$2[Cu(II)OH]^+ \rightarrow Cu(I) + [Cu(II)O]^+ + H_2O$$
 (18)

There is a dearth of experimental evidence for [Cu(II)O] ⁺ on Cu-zeolites, and DFT-computed formation free energies of [Cu(II)O] ⁺ species are unfavorable compared to binuclear and larger Cu clusters. ³¹ Therefore, we conclude that plausible Cu(II) auto-reduction mechanisms must comprise elementary steps (such as the reverse of Eq. 10) that can rationalize both the observed increase in auto-reducible Cu sites on samples of higher ZCuOH density and the observation that a smaller fraction of binuclear Cu sites are able to undergo auto-reduction than reduction in CO.

3.4. Influence of Cu Speciation and Density on the Fraction of Sites Reducible by Methane

To provide a quantitative link between the extent of Cu²⁺ autoreduction in inert (723 K) and in CH₄ (473 K) treatments, the same three Cu-CHA samples of varying ZCuOH density (samples C, D, and A) were O₂ activated at high temperature treatments (21 kPa, 723 K, 2 h) and then exposed to CH₄ (4.1 kPa CH₄, 473 K, up to 2 h). In situ XANES data are shown in Figures 7d-f, with the Cu²⁺ and Cu⁺ fractions shown in Table 2. First, a small amount of Cu(II) reduction was observed on the Z₂Cu-containing control sample (37% Cu(I), Sample C, Table 2). The extent of Cu²⁺ reduction increased with the nominal ZCuOH site density (86% Cu⁺ on Sample D to 92% Cu⁺ on Sample A; Table 2). For Samples D and A, these values were similar to the Cu⁺ quantified after auto-reduction (Table 2). These data suggest a quantitative link between the binuclear Cu structures involved in both CH₄-reduction and He auto-reduction pathways, implicating Cu-O₂-Cu sites, but not Cu-O-Cu sites, are the active sites for stoichiometric PMO cycles under the conditions studied here. These data provide further support for using the number of auto-reducible Cu(II) sites to normalize methanol yields formed from stoichiometric PMO cycles, as done previously.^{1,2}

In Section 3.3, UV-Vis spectra are shown in Figure 8 for sample A after exposure to similar treatments as used in the stoichiometric PMO cycle. After high-temperature O2 activation (Fig. 8, black), subsequent exposure to CH₄ (Fig. 8, blue) led to a partial decrease in d-d transition (~8,000–16,000 cm⁻¹) and LMCT bands (~24,000–30,000 cm $^{-1}$) attributed to various O/O₂-bridged binuclear Cu species. 11,13,16,31,74 After CH₄ exposure, the UV-Vis bands remain in the d-d transition and low-energy LMCT region, indicating some fraction of binuclear Cu sites and isolated ZCuOH that are not reduced to Cu⁺ by CH₄ and thus would not participate in stoichiometric PMO cycles under these conditions. Therefore, CH₄ appears to reduce only a partial fraction of the O/O2-bridged binuclear Cu species present to likely form methoxy-bridged structures (i.e., Cu⁺-OCH₃-Cu⁺ or Cu⁺-OCH₃-OH-Cu⁺) that have been invoked previously in PMO reaction schemes. 6,23 Given the similar UV-Vis spectra measured after auto-reduction and CH₄-reduction (Fig. 8), we propose both treatments reduce a common binuclear Cu structure (i.e., Cu-O₂-Cu). The UV-Vis spectrum collected following a subsequent CO reduction treatment resulted in complete disappearance of all features attributable to O/O2-bridged binuclear Cu species (Fig. 8, light grey), indicating that CO reduces a greater fraction of the Cu present (likely, Cu-O-Cu) than CH₄ and He.

To explore the thermodynamics of stoichiometric PMO reduction steps, we computed Cu(II) reduction reaction free energies at methane reduction conditions (473 K, 21×10^{-4} kPa of O₂, 0.01% of H₂O, 4.1 kPa of CH₄, 1 bar total pressure) according to:

 $Z_2Cu_2H_xO_v + yCH_4$

$$ZCuOH + CH_4 + \frac{1}{4}O_2 \rightarrow ZCu + CH_3OH + \frac{1}{2}H_2O$$
 (20)

These reaction energies were computed for the same binuclear Cu structures and the same six Al pair configurations as examined for auto-reduction (Fig. 9a), as well as for mononuclear ZCuOH, as shown in Figure 9b. Mononuclear ZCuOH sites are predicted to reduce to Cu(I) at these conditions, consistent with proposals that ZCuOH may act as an active site for the PMO reaction, 9,10 although elementary steps describing such a mechanism are lacking. Like auto-reduction reaction energies (Fig. 9a), various binuclear Cu structures exhibit varying thermodynamic preferences for reduction in methane. Mono- $(\mu$ -oxo)dicopper and mono- $(\mu$ -hydroxyl)dicopper are predicted to be slightly unstable (-10 kJ mol⁻¹) to slightly stable (40 kJ mol⁻¹) against CH₄ reduction, similar to findings reported by Engedahl et al., 79 while O2 and (OH)2-bridged structures are expected to be reducible by CH₄ at these conditions. The similar DFT-predicted thermodynamic tendencies of Cu structures to undergo auto-reduction and CH₄ reduction rationalize the similar extent of Cu²⁺ reduction found experimentally (Table 2), suggesting that O₂ and/or (OH)₂-bridged sites serve as dominant active sites in Cu-CHA for methane oxidation at the conditions studied.

3.5. Proposed Active Sites and Elementary Steps for Partial Methane Oxidation to Methanol

The changes to Cu structures and oxidation states, based on experimental observations upon exposure of Cu-CHA zeolites to Cu(II) reduction treatments of increasing severity, are depicted in Scheme 2. The first step in the stoichiometric PMO cycle is a high temperature oxidation treatment (e.g., 723 K), in which in situ XAS, UV-Visible, and Raman spectroscopies together provide evidence for a mixture of isolated Z₂Cu and ZCuOH, mono-(μ -oxo) dicopper either isolated or in proximity to another mono- $(\mu$ -oxo) dicopper, O₂-bridged species (e.g., trans-\u03c4-1,2-peroxo dicopper), along with a minority amount of isolated Cu⁺ species (Scheme 2a). This experimental evidence also supports DFT calculations for different Al-Al pair distributions in Cu-CHA that show the presence of multiple Cu species (Fig. 2), wherein some binuclear Cu structures (mono-(µ-oxo) dicopper) form upon condensation of two proximal ZCuOH.67,78 The exact distributions of these Cu structures and their proximity depend on the density and arrangement of extraframework Cu and framework Al sites, and on the O2-activation conditions used, as illustrated in Figure 2.

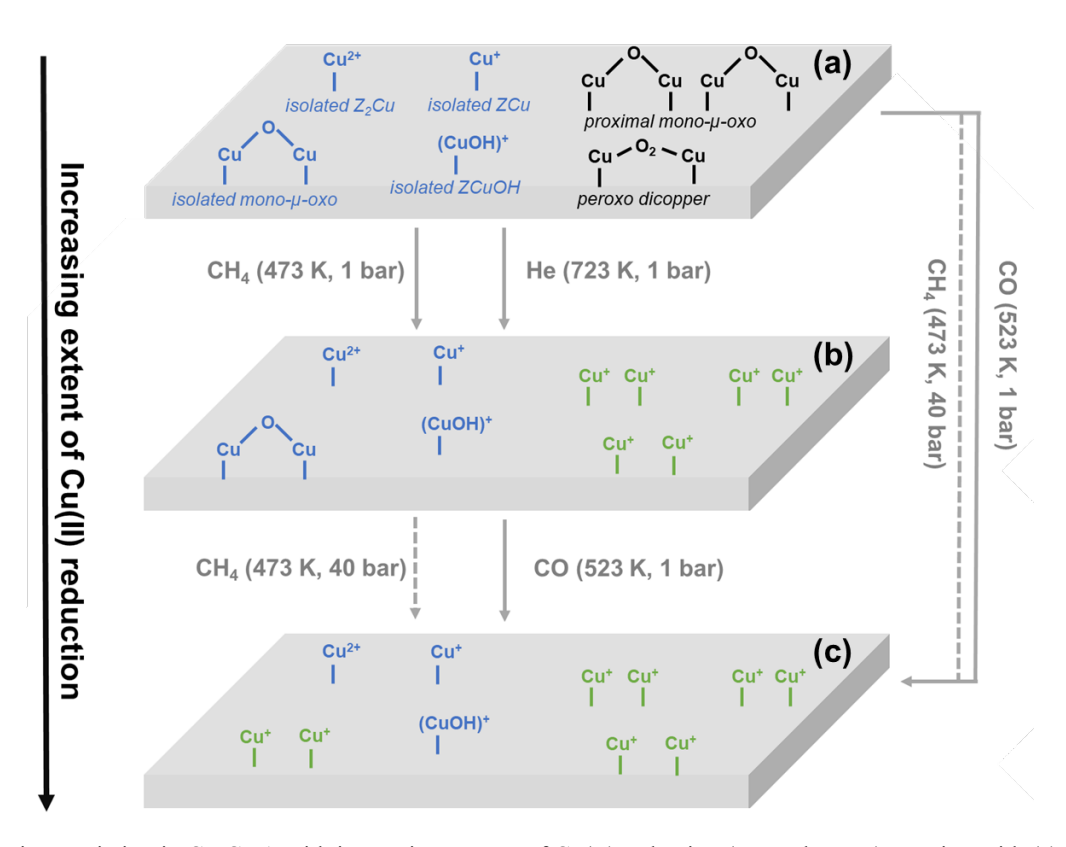
The next step in the stoichiometric PMO cycle is exposure in CH₄ at moderate temperatures and pressures (1 bar, 473 K), which results in partial Cu²⁺ reduction to Cu⁺ in quantities that identical to the extent of auto-reduction that occurs under high-temperature inert environments (He, 723 K; Table 2). Elementary steps that describe Cu²⁺ auto-reduction can be written for a O₂-bridged species (the reverse of Eq. 10), but not for isolated ZCuOH, Z₂Cu, or mono-(µ-oxo) dicopper sites, so these sites are depicted as remaining in the Cu²⁺ state in Scheme 2b. Auto-reducible binuclear Cu species can exist as a pool of Cu sites, some of which contain Cu(II) auto-reduction pathways that evolve O₂. ZCuO₂CuZ sites can plausibly auto-reduce through elimination of O₂. Similarly, two ZCuOCuZ sites of sufficient, but at this point unknown, proximity may undergo auto-reduction to eliminate O₂. An isolated ZCuOCuZ site, in contrast, has no evident pathway for auto-reduction. The more

likely auto-reduction pathway would appear to involve a single O₂-bridged Cu site following the reverse of Eq.10, given the requirement of 2 Cu rather than 4 Cu sites in close proximity to complete the elementary steps required. We note there are other complexities during auto-reduction, including the presence of water⁸⁰ or surface carbonaceous debris facilitating alternate Cu²⁺ reduction pathways,⁷⁸ which we discount given the evidence supporting reverse of Eq. 10 as the likely pathway for auto-reduction.

More aggressive reduction treatments (CO, 523 K) result in further extents of Cu²⁺ reduction, specifically the remaining bridged Cu-O_x-Cu species, but not isolated Z₂Cu and ZCuOH sites as shown by Li et al., 31 which is consistent with the CO-assisted reduction of the isolated mono- $(\mu$ -oxo) dicopper species (via Eq. 13) that remain on Cu-CHA samples following auto-reduction (He, 723 K) or low-pressure CH₄ reduction (1 bar, 473 K), as portrayed in Scheme 2c. CO reduces all O_x-bridged Cu structures, leading to the over-estimation of Cu sites that participate in stoichiometric PMO cycles (Table S2, SI), providing further support to normalize methanol yields (473 K, 1 bar) by the amount of auto-reducible Cu. 1,2,81 Scheme 2 also shows pathways depicted by dashed arrows that we surmise should occur, based on prior literature evidence, that higher CH₄ pressures (40 bar, 473 K) result in higher methanol yields (per Cu) from stoichiometric PMO cycles, 2,26 implying that higher CH₄ pressures provide sufficient driving force to reduce all Cu-O_x-Cu species formed after O₂-activation of the sample.

The bound *CH₃ species formed after CH₄-reduction of O_xbridged Cu active sites can be quantified as methanol, as well as over-oxidation products (CO, CO₂), in subsequent water extraction steps to complete the stoichiometric PMO reaction, assuming that each O species in the Cu complex reacts to form one methanol.^{6,16} These measurements were performed on a much larger suite of Cu-CHA samples than spectroscopic data were measured on, to assess trends in PMO yields for a family of materials of widely varying Cu density and speciation, as shown in Figure 10a, Control Cu-CHA samples containing predominantly Z₂Cu sites (samples B and C, Table 1) did not form methanol after a stoichiometric PMO cycle, consistent with Pappas et al. 1 Methanol yields (per Cu) do not depend systematically on total Cu content (Fig. S30a, SI), because several properties vary simultaneously among these samples, including Al density and arrangement, that cause variations in Cu²⁺ speciation. Instead, methanol yields increase generally with increasing ZCuOH spatial density (plotted as ZCuOH per cage in Fig. 10a). Furthermore, using the phase diagrams (Fig. 2) to predict binuclear Cu site content, Fig. 10b shows that methanol yields (per Cu) generally increase with binuclear Cu site content (per Cu), in samples with mixtures of mononuclear and binuclear Cu species. The amount of methanol formed (per Cu) is not a single-valued function of binuclear Cu site content, however, as some materials predicted to have similar fraction of binuclear Cu sites yield significantly different amounts of methanol. This reflects both limitations of the thermodynamic assumptions that underlie the phase diagrams in Fig. 2, and that binuclear Cu sites comprise a pool of structures with varying reactivity (Fig. 9b) that might be influenced by Al location. These differences are highlighted by differences in reactivity with CO and CH₄, as shown in Table S2,

Stoichiometric PMO yields and the number of binuclear O_x -bridged sites formed after O_2 activation (per Cu) both depend on ZCuOH density (ZCuOH/cage) on a given Cu-CHA sample, indicating that materials with higher ZCuOH content and sites closer in proximity form more PMO-active sites. Specifically, these data indicate that the same subset of Cu^{2+} sites undergo auto-reduction (723 K) and reduction by CH₄ (473 K), which we propose are binuclear O_2 -bridged binuclear Cu species (Eq. 19) or two proximal O-bridged binuclear Cu species (Eq. 19) that are capable of both releasing O_2 in auto-reduction steps and forming methoxy species from reaction with CH₄. The latter is consistent with Dinh et al.



Scheme 2. Cu site speciation in Cu-CHA with increasing extents of Cu(II) reduction (top-to-bottom), starting with (a) high-temperature oxidation (O₂, 723 K), (b) auto-reduction in inert (He, 723 K) or reduction in low-pressure methane (CH₄, 1 bar, 473 K), (c) reduction in CO (1 bar, 523 K) or high-pressure methane (CH₄, 40 bar, 473); solid arrows supported by data in this study, dashed arrows speculated based on prior literature reports.

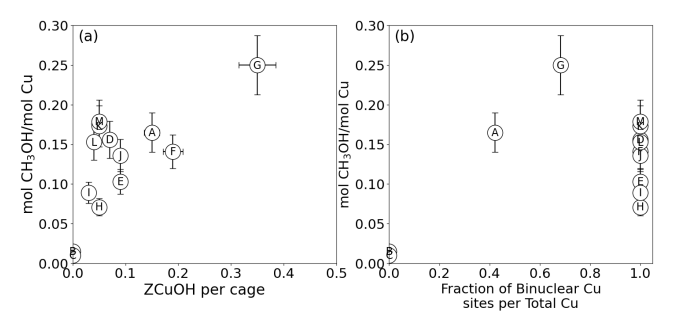
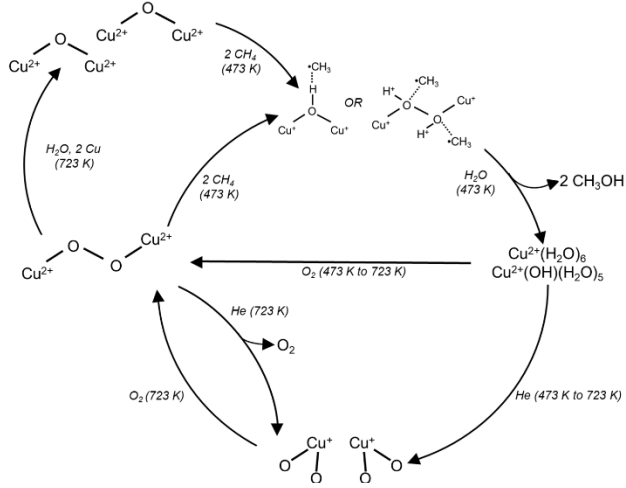


Figure 10. Stoichiometric PMO yields to methanol as a function of (a) ZCuOH per cage and (b) fraction of binuclear Cu sites (per total Cu) determined using titration model in Fig. 2 and Table 1.

We further note that *trans-μ*-1,2-peroxo dicopper (and O₂-bridged dicopper sites, generally) can convert into more stable *mono-μ*-oxo dicopper sites, and at faster rates in the presence of water.⁴³ These dicopper site interconversions are depicted in proposed reaction cycles for PMO in Scheme 3, which is consistent with the data presented herein that a common pool of Cu active sites for both CH₄-reduction and auto-reduction comprise both O₂-bridged dicopper sites or two proximal O-bridged dicopper sites. Scheme 3 displays a mechanism for PMO at extra-lattice oxygen species contained within this pool of ZCuO₂CuZ and proximal ZCuOCuZ species, with an elementary step to connect this pool of

PMO-active Cu species to high-temperature auto-reduction events (He, 723 K).



Scheme 3. Proposed stoichiometric PMO reaction cycles over Cu-O₂-Cu sites or proximal Cu-O-Cu sites that can interconvert from Cu-O₂-Cu species.

Upon high-temperature oxidation treatment, Cu-CHA zeolites form a mixture of O and O_2 -bridged binuclear Cu species⁴³ as well as isolated Z_2 Cu, ZCuOH, and isolated ZCuOCuZ species that are

spectators in the PMO cycle (at 1 bar CH₄, 473 K). Two proximal O-bridged Cu species, or one O2-bridged Cu species, can either auto-reduce to $Cu(I)^{1,2,16}$ or be reduced by methane to form methanol, likely via radical-rebound type mechanisms proposed previously.^{23,84} Proximal ZCuOCuZ sites would result in CH₃OH/Cu = 0.5 stoichiometry, while ZCuO2CuZ sites would result in CH₃OH/Cu = 1, without accounting for over-oxidation products (i.e., HCHO, CO, CO₂); typically, these theoretical yields are achieved by varying reaction conditions (e.g., increasing CH₄ pressure).² In order for methanol to form, water must be introduced (473 K, 2.5 kPa H₂O) to react with the bound methoxy species;⁵ moreover, hydrated mononuclear Cu(II) species should form as products of this step, based on in situ XAS (Figs. S27-S28, SI), UV-Vis spectra, and DFT-predicted phase diagrams.³⁸ This detail of forming hydrated mononuclear Cu(II) sites and their requirement to convert back into binuclear Ox-bridged Cu structures has not been explicitly considered in prior PMO cycles, but likely occur by pathways analogous to those occurring when a Cu²⁺-exchanged zeolite sample is initially exposed to an O₂-activation treatment. ^{1,26}

4. Conclusions

The identities of active Cu sites for stoichiometric PMO in Cuzeolites remain debated, in part because the Cu species that form depend strongly on pressure and temperature as well as microscopic features of the zeolite support, including the framework Al density and distribution. Experimental and theoretical evidence show that various binuclear O-/O2-bridged Cu structures form after oxidation treatments of Cu-CHA samples of varying composition, especially those containing high densities of nominally ZCuOH sites. The free energies of various mononuclear and binuclear sites depend strongly on partial pressures and temperature, as well as the specific configurations of Al atoms in the zeolite lattice. The latter details are often overlooked in theoretical assessments of metal cations and complexes exchanged onto zeolite supports but are required for accurate interpretations of experimental observations.

Thermodynamic and kinetic factors cause a mixture of O₂bridged Cu active site structures to formed on Cu-CHA after hightemperature O₂ activation treatments. An identical fraction of Cu²⁺ sites auto-reduce under high-temperature inert environments (723 K, He) and are reduced by methane at lower temperatures (473 K, 1 bar CH₄), implicating O₂-bridged dicopper(II) species as a likely common intermediate. In contrast, a larger fraction of Cu sites are reduced by CO (523 K, 1 bar), likely isolated mono-(μ-oxo)dicopper(II) species. These observations support using the number of auto-reducible Cu²⁺ sites on a given Cu-zeolite to normalize methanol yields from stoichiometric PMO cycles (473 K, 1 bar CH₄); additional Cu species likely participate in stoichiometric PMO at higher CH₄ pressures. Complete auto-reduction or CH₄-reduction of Cu(II) sites was not observed on any Cu-CHA sample studied here, motivating continued research to tailor material synthesis routes to increase the fraction of Cu sites that can be utilized in the stoichiometric PMO reaction cycle.

In stoichiometric PMO cycles on Cu-CHA, methanol yields (per Cu) generally increased with the number of binuclear O_x-bridged Cu sites predicted from theoretical phase diagrams. The variation in O_x-bridged dicopper structures, and in their stabilities and reaction energies toward CH₄-reduction, preclude establishing a more quantitative link between the number of such sites and methanol yields from PMO. Our observations motivate adding three important details to the stoichiometric PMO reaction mechanisms postulated in prior literature. First, both O₂-bridged and O-bridged dicopper species are in the pool of active sites. Second, elementary steps for O₂ activation and auto-reduction require that the mono-(*µ*-oxo)dicopper(II) sites be present as pairs in sufficiently close proximity, implicating a total of 4 Cu sites to close the PMO cycle. Third, after CH₄-activated samples are exposed to water (473)

K) to extract methanol, Cu ions are present as isolated, hydrated species, and further site restructuring must occur upon oxidative treatments to form the binuclear O_x -bridged Cu sites that participate in the next PMO cycle. These findings motivate further research into the mechanistic details of O_2 -activation of Cu sites in Cu-zeolites and their reactivity towards oxidizing CH_4 , and its reaction product (CH_3OH).

AUTHOR INFORMATION

Corresponding Author

William F. Schneider: <u>wschneider@nd.edu</u> Rajamani Gounder: <u>rgounder@purdue.edu</u>

Author Contributions

[†]L. N. W. and J. R.-O. contributed equally to this work.

Notes

The authors declare no competing financial interests.

ASSOCIATED CONTENT

Supporting Information

Cu-CHA characterization, estimates of Cu per CHA cage, UV-Visible spectra, Raman spectra, CO temperature programmed reduction data, X-ray absorption spectra, stoichiometric partial methane oxidation yields, DFT energies and vibrational frequencies of Cu species, comparisons between free energy calculations, simulated phase diagrams of Cu-CHA for different Al and Cu siting (PDF)

Geometries of all computed species provided in a file (ZIP)

ACKNOWLEDGMENT

The experimental work at Purdue University on zeolite synthesis and characterization was supported by the U.S. Department of Energy, Office of Science, Office of Basic Energy Sciences, under Award Number DE-SC0019026. Use of the Advanced Photon Source is supported by the U.S. Department of Energy, Office of Science, and Office of Basic Energy Sciences, under Contract no. DE-AC02-06CH11357. MRCAT operations and beamline 10-ID are supported by the Department of Energy and the MRCAT member institutions. The computational work at Notre Dame was supported by the National Science Foundation CBET-DMREF program under award number 1922154. The computing resources were provided by the Notre Dame Center for Research Computing. We also thank Sachem, Inc. for providing the organic structure-directing agent used to synthesize CHA. We acknowledge technical discussions with Prof. Jeffrey Miller and Dr. Nicole LiBretto (Purdue) for XAS data analysis and fitting, and Prof. Christopher Paolucci (Virginia) for discussion of the DFT results. We also acknowledge Lauren Kilburn (Purdue) for technical discussions and a careful review of the manuscript.

REFERENCES

- (1) Pappas, D. K.; Borfecchia, E.; Dyballa, M.; Pankin, I. A.; Lomachenko, K. A.; Martini, A.; Signorile, M.; Teketel, S.; Arstad, B.; Berlier, G.; Lamberti, C.; Bordiga, S.; Olsbye, U.; Lillerud, K. P.; Svelle, S.; Beato, P. Methane to Methanol: Structure–Activity Relationships for Cu-CHA. *J. Am. Chem. Soc.* **2017**, *139* (42), 14961–14975. https://doi.org/10.1021/jacs.7b06472.
- (2) Brezicki, G.; Kammert, J. D.; Gunnoe, T. B.; Paolucci, C.; Davis, R. J. Insights into the Speciation of Cu in the Cu-H-Mordenite Catalyst for the Oxidation of Methane to Methanol. *ACS Catal.* **2019**, *9* (6), 5308–5319. https://doi.org/10.1021/acscatal.9b00852.
- (3) Grundner, S.; Markovits, M. A. C.; Li, G.; Tromp, M.; Pidko, E. A.; Hensen, E. J. M.; Jentys, A.; Sanchez-Sanchez, M.; Lercher, J. A. Single-Site Trinuclear Copper Oxygen Clusters in Mordenite for Selective

- Conversion of Methane to Methanol. *Nat. Commun.* **2015**, *6* (1), 7546. https://doi.org/10.1038/ncomms8546.
- (4) Alayon, E. M. C.; Nachtegaal, M.; Ranocchiari, M.; van Bokhoven, J. a. Catalytic Conversion of Methane to Methanol Using Cu-Zeolites. *Chimia* **2012**, *66* (9), 668–674. https://doi.org/10.2533/chimia.2012.668.
- (5) Narsimhan, K.; Iyoki, K.; Dinh, K.; Román-Leshkov, Y. Catalytic Oxidation of Methane into Methanol over Copper-Exchanged Zeolites with Oxygen at Low Temperature. *ACS Cent. Sci.* **2016**, *2* (6), 424–429. https://doi.org/10.1021/acscentsci.6b00139.
- (6) Dinh, K. T.; Sullivan, M. M.; Narsimhan, K.; Serna, P.; Meyer, R. J.; Dincă, M.; Román-Leshkov, Y. Continuous Partial Oxidation of Methane to Methanol Catalyzed by Diffusion-Paired Copper Dimers in Copper-Exchanged Zeolites. *J. Am. Chem. Soc.* **2019**, *141* (29), 11641–11650. https://doi.org/10.1021/jacs.9b04906.
- (7) Ohyama, J.; Tsuchimura, Y.; Hirayama, A.; Iwai, H.; Yoshida, H.; Machida, M.; Nishimura, S.; Kato, K.; Takahashi, K. Relationships among the Catalytic Performance, Redox Activity, and Structure of Cu-CHA Catalysts for the Direct Oxidation of Methane to Methanol Investigated Using *In Situ* XAFS and UV-Vis Spectroscopies. *ACS Catal.* **2022**, *12* (4), 2454–2462. https://doi.org/10.1021/acscatal.1c05559.
- (8) Tsuchimura, Y.; Yoshida, H.; Machida, M.; Nishimura, S.; Takahashi, K.; Ohyama, J. Investigation of the Active-Site Structure of Cu-CHA Catalysts for the Direct Oxidation of Methane to Methanol Using In Situ UV-Vis Spectroscopy. *Energy Fuels* **2023**, *37* (13), 9411–9418. https://doi.org/10.1021/acs.energyfuels.3c00333.
- (9) Kulkarni, A. R.; Zhao, Z.-J.; Siahrostami, S.; Nørskov, J. K.; Studt, F. Monocopper Active Site for Partial Methane Oxidation in Cu-Exchanged 8MR Zeolites. *ACS Catal.* **2016**, *6* (10), 6531–6536. https://doi.org/10.1021/acscatal.6b01895.
- (10) Sushkevich, V. L.; Artsiusheuski, M.; Klose, D.; Jeschke, G.; Bokhoven, J. A. Identification of Kinetic and Spectroscopic Signatures of Copper Sites for Direct Oxidation of Methane to Methanol. *Angew. Chem. Int. Ed.* **2021**, *60* (29), 15944–15953. https://doi.org/10.1002/anie.202101628.
- (11) Groothaert, M. H.; van Bokhoven, J. A.; Battiston, A. A.; Weckhuysen, B. M.; Schoonheydt, R. A. Bis(μ-Oxo)Dicopper in Cu-ZSM-5 and Its Role in the Decomposition of NO: A Combined in Situ XAFS, UV-Vis-Near-IR, and Kinetic Study. *J. Am. Chem. Soc.* **2003**, *125* (25), 7629–7640. https://doi.org/10.1021/ja029684w.
- (12) Groothaert, M. H.; Smeets, P. J.; Sels, B. F.; Jacobs, P. A.; Schoonheydt, R. A. Selective Oxidation of Methane by the Bis(μ-Oxo)Dicopper Core Stabilized on ZSM-5 and Mordenite Zeolites. *J. Am. Chem. Soc.* **2005**, *127* (5), 1394–1395. https://doi.org/10.1021/ja047158u.
- (13) Woertink, J. S.; Smeets, P. J.; Groothaert, M. H.; Vance, M. A.; Sels, B. F.; Schoonheydt, R. A.; Solomon, E. I. A $[Cu\ _2\ O]\ ^{2+}$ Core in Cu-ZSM-5, the Active Site in the Oxidation of Methane to Methanol. *Proc. Natl. Acad. Sci.* **2009**, *106* (45), 18908–18913. https://doi.org/10.1073/pnas.0910461106.
- (14) Alayon, E. M. C.; Nachtegaal, M.; Bodi, A.; Ranocchiari, M.; van Bokhoven, J. A. Bis(μ-Oxo) versus Mono(μ-Oxo)Dicopper Cores in a Zeolite for Converting Methane to Methanol: An in Situ XAS and DFT Investigation. *Phys. Chem. Chem. Phys.* **2015**, *17* (12), 7681–7693. https://doi.org/10.1039/C4CP03226H.
- (15) Ipek, B.; Wulfers, M. J.; Kim, H.; Göltl, F.; Hermans, I.; Smith, J. P.; Booksh, K. S.; Brown, C. M.; Lobo, R. F. Formation of [Cu $_2$ O $_2$] $^{2+}$ and [Cu $_2$ O] $^{2+}$ toward C–H Bond Activation in Cu-SSZ-13 and Cu-SSZ-39. *ACS Catal.* **2017**, 7 (7), 4291–4303. https://doi.org/10.1021/acscatal.6b03005.
- (16) Brezicki, G.; Zheng, J.; Paolucci, C.; Schlögl, R.; Davis, R. J. Effect of the Co-Cation on Cu Speciation in Cu-Exchanged Mordenite and ZSM-5 Catalysts for the Oxidation of Methane to Methanol. *ACS Catal.* **2021**, *11* (9), 4973–4987. https://doi.org/10.1021/acscatal.1c00543.
- (17) Rhoda, H. M.; Plessers, D.; Heyer, A. J.; Bols, M. L.; Schoonheydt, R. A.; Sels, B. F.; Solomon, E. I. Spectroscopic Definition of a Highly Reactive Site in Cu-CHA for Selective Methane Oxidation: Tuning a Mono-μ-Oxo Dicopper(II) Active Site for Reactivity. *J. Am. Chem. Soc.* **2021**, *143* (19), 7531–7540. https://doi.org/10.1021/jacs.1c02835.
- (18) Nachtigall, P.; Arean, C. O. Themed Issue on Characterization of Adsorbed Species. *Phys. Chem. Chem. Phys.* **2010**, *12* (24), 6307. https://doi.org/10.1039/c0cp90026e.
- (19) Knorpp, A. J.; Pinar, A. B.; Baerlocher, C.; McCusker, L. B.; Casati, N.; Newton, M. A.; Checchia, S.; Meyet, J.; Palagin, D.; Bokhoven, J. A. Paired Copper Monomers in Zeolite Omega: The Active Site for

- Methane-to-Methanol Conversion. *Angew. Chem.* **2021**, *133* (11), 5918–5922. https://doi.org/10.1002/ange.202014030.
- (20) Göltl, F.; Bhandari, S.; Mavrikakis, M. Thermodynamics Perspective on the Stepwise Conversion of Methane to Methanol over Cu-Exchanged SSZ-13. *ACS Catal.* **2021**, *11* (13), 7719–7734. https://doi.org/10.1021/acscatal.1c00691.
- (21) Göltl, F.; Bhandari, S.; Lebrón-Rodríguez, E. A.; Gold, J. I.; Zones, S. I.; Hermans, I.; Dumesic, J. A.; Mavrikakis, M. Identifying Hydroxylated Copper Dimers in SSZ-13 via UV-Vis-NIR Spectroscopy. *Catal. Sci. Technol.* **2022**, *12* (9), 2744–2748. https://doi.org/10.1039/D2CY00353H.
- (22) Grundner, S.; Luo, W.; Sanchez-Sanchez, M.; Lercher, J. A. Synthesis of Single-Site Copper Catalysts for Methane Partial Oxidation. *Chem. Commun.* **2016**, *52* (12), 2553–2556. https://doi.org/10.1039/C5CC08371K.
- (23) Li, G.; Vassilev, P.; Sanchez-Sanchez, M.; Lercher, J. A.; Hensen, E. J. M.; Pidko, E. A. Stability and Reactivity of Copper Oxo-Clusters in ZSM-5 Zeolite for Selective Methane Oxidation to Methanol. *J. Catal.* **2016**, *338*, 305–312. https://doi.org/10.1016/j.jcat.2016.03.014.
- (24) Palagin, D.; Knorpp, A. J.; Pinar, A. B.; Ranocchiari, M.; van Bokhoven, J. A. Assessing the Relative Stability of Copper Oxide Clusters as Active Sites of a CuMOR Zeolite for Methane to Methanol Conversion: Size Matters? *Nanoscale* **2017**, *9* (3), 1144–1153. https://doi.org/10.1039/C6NR07723D.
- (25) Newton, M. A.; Knorpp, A. J.; Sushkevich, V. L.; Palagin, D.; van Bokhoven, J. A. Active Sites and Mechanisms in the Direct Conversion of Methane to Methanol Using Cu in Zeolitic Hosts: A Critical Examination. *Chem. Soc. Rev.* **2020**, *49* (5), 1449–1486. https://doi.org/10.1039/C7CS00709D.
- (26) Tomkins, P.; Mansouri, A.; Bozbag, S. E.; Krumeich, F.; Park, M. B.; Alayon, E. M. C.; Ranocchiari, M.; van Bokhoven, J. A. Isothermal Cyclic Conversion of Methane into Methanol over Copper-Exchanged Zeolite at Low Temperature. *Angew. Chem. Int. Ed.* **2016**, *55* (18), 5467–5471. https://doi.org/10.1002/anie.201511065.
- (27) Vanelderen, P.; Snyder, B. E. R.; Tsai, M.-L.; Hadt, R. G.; Vancauwenbergh, J.; Coussens, O.; Schoonheydt, R. A.; Sels, B. F.; Solomon, E. I. Spectroscopic Definition of the Copper Active Sites in Mordenite: Selective Methane Oxidation. *J. Am. Chem. Soc.* **2015**, *137* (19), 6383–6392. https://doi.org/10.1021/jacs.5b02817.
- (28) Pappas, D. K.; Martini, A.; Dyballa, M.; Kvande, K.; Teketel, S.; Lomachenko, K. A.; Baran, R.; Glatzel, P.; Arstad, B.; Berlier, G.; Lamberti, C.; Bordiga, S.; Olsbye, U.; Svelle, S.; Beato, P.; Borfecchia, E. The Nuclearity of the Active Site for Methane to Methanol Conversion in Cu-Mordenite: A Quantitative Assessment. *J. Am. Chem. Soc.* **2018**, *140* (45), 15270–15278. https://doi.org/10.1021/jacs.8b08071.
- (29) Deplano, G.; Martini, A.; Signorile, M.; Borfecchia, E.; Crocellà, V.; Svelle, S.; Bordiga, S. Copper Pairing in the Mordenite Framework as a Function of the Cu ¹/Cu ^{II} Speciation. *Angew. Chem. Int. Ed.* **2021**, *60* (49), 25891–25896. https://doi.org/10.1002/anie.202109705.
- (30) Pankin, I. A.; Martini, A.; Lomachenko, K. A.; Soldatov, A. V.; Bordiga, S.; Borfecchia, E. Identifying Cu-Oxo Species in Cu-Zeolites by XAS: A Theoretical Survey by DFT-Assisted XANES Simulation and EXAFS Wavelet Transform. *Catal. Today* **2020**, *345*, 125–135. https://doi.org/10.1016/j.cattod.2019.09.032.
- (31) Li, H.; Paolucci, C.; Khurana, I.; N. Wilcox, L.; Göltl, F.; D. Albarracin-Caballero, J.; J. Shih, A.; H. Ribeiro, F.; Gounder, R.; F. Schneider, W. Consequences of Exchange-Site Heterogeneity and Dynamics on the UV-Visible Spectrum of Cu-Exchanged SSZ-13. *Chem. Sci.* **2019**, *10* (8), 2373–2384. https://doi.org/10.1039/C8SC05056B.
- (32) Borfecchia, E.; Beato, P.; Svelle, S.; Olsbye, U.; Lamberti, C.; Bordiga, S. Cu-CHA a Model System for Applied Selective Redox Catalysis. *Chem. Soc. Rev.* **2018**, *47* (22), 8097–8133. https://doi.org/10.1039/C8CS00373D.
- (33) Paolucci, C.; Di Iorio, J. R.; Ribeiro, F. H.; Gounder, R.; Schneider, W. F. Catalysis Science of NOx Selective Catalytic Reduction With Ammonia Over Cu-SSZ-13 and Cu-SAPO-34. In *Advances in Catalysis*; Elsevier, 2016; Vol. 59, pp 1–107. https://doi.org/10.1016/bs.acat.2016.10.002.
- (34) Godiksen, A.; Stappen, F. N.; Vennestrøm, P. N. R.; Giordanino, F.; Rasmussen, S. B.; Lundegaard, L. F.; Mossin, S. Coordination Environment of Copper Sites in Cu-CHA Zeolite Investigated by Electron Paramagnetic Resonance. *J. Phys. Chem. C* **2014**, *118* (40), 23126–23138. https://doi.org/10.1021/jp5065616.
- (35) Bols, M. L.; Hallaert, S. D.; Snyder, B. E. R.; Devos, J.; Plessers, D.; Rhoda, H. M.; Dusselier, M.; Schoonheydt, R. A.; Pierloot, K.;

- Solomon, E. I.; Sels, B. F. Spectroscopic Identification of the α -Fe/ α -O Active Site in Fe-CHA Zeolite for the Low-Temperature Activation of the Methane C–H Bond. *J. Am. Chem. Soc.* **2018**, *140* (38), 12021–12032. https://doi.org/10.1021/jacs.8b05877.
- (36) Li, S.; Wang, Y.; Wu, T.; Schneider, W. F. First-Principles Analysis of Site- and Condition-Dependent Fe Speciation in SSZ-13 and Implications for Catalyst Optimization. *ACS Catal.* **2018**, *8* (11), 10119–10130. https://doi.org/10.1021/acscatal.8b02107.
- (37) Devos, J.; Bols, M. L.; Plessers, D.; Goethem, C. V.; Seo, J. W.; Hwang, S.-J.; Sels, B. F.; Dusselier, M. Synthesis–Structure–Activity Relations in Fe-CHA for C–H Activation: Control of Al Distribution by Interzeolite Conversion. *Chem. Mater.* **2020**, *32* (1), 273–285. https://doi.org/10.1021/acs.chemmater.9b03738.
- (38) Paolucci, C.; Parekh, A. A.; Khurana, I.; Di Iorio, J. R.; Li, H.; Albarracin Caballero, J. D.; Shih, A. J.; Anggara, T.; Delgass, W. N.; Miller, J. T.; Ribeiro, F. H.; Gounder, R.; Schneider, W. F. Catalysis in a Cage: Condition-Dependent Speciation and Dynamics of Exchanged Cu Cations in SSZ-13 Zeolites. *J. Am. Chem. Soc.* **2016**, *138* (18), 6028–6048. https://doi.org/10.1021/jacs.6b02651.
- (39) Di Iorio, J. R.; Gounder, R. Controlling the Isolation and Pairing of Aluminum in Chabazite Zeolites Using Mixtures of Organic and Inorganic Structure-Directing Agents. *Chem. Mater.* **2016**, *28* (7), 2236–2247. https://doi.org/10.1021/acs.chemmater.6b00181.
- (40) Di Iorio, J. R.; Li, S.; Jones, C. B.; Nimlos, C. T.; Wang, Y.; Kunkes, E.; Vattipalli, V.; Prasad, S.; Moini, A.; Schneider, W. F.; Gounder, R. Cooperative and Competitive Occlusion of Organic and Inorganic Structure-Directing Agents within Chabazite Zeolites Influences Their Aluminum Arrangement. *J. Am. Chem. Soc.* **2020**, *142* (10), 4807–4819. https://doi.org/10.1021/jacs.9b13817.
- (41) Wang, X.; Wang, Y.; Moini, A.; Gounder, R.; Maginn, E. J.; Schneider, W. F. Influence of an N, N, N-Trimethyl-1-Adamantyl Ammonium (TMAda ⁺) Structure Directing Agent on Al Distributions and Pair Features in Chabazite Zeolite. *Chem. Mater.* **2022**, *34* (24), 10811–10822. https://doi.org/10.1021/acs.chemmater.2c01465.
- (42) Lee, S.; Nimlos, C. T.; Kipp, E. R.; Wang, Y.; Gao, X.; Schneider, W. F.; Lusardi, M.; Vattipalli, V.; Prasad, S.; Moini, A.; Gounder, R. Evolution of Framework Al Arrangements in CHA Zeolites during Crystallization in the Presence of Organic and Inorganic Structure-Directing Agents. *Cryst. Growth Des.* **2022**, *22* (10), 6275–6295. https://doi.org/10.1021/acs.cgd.2c00856.
- (43) Bregante, D. T.; Wilcox, L. N.; Liu, C.; Paolucci, C.; Gounder, R.; Flaherty, D. W. Dioxygen Activation Kinetics over Distinct Cu Site Types in Cu-Chabazite Zeolites. *ACS Catal.* **2021**, *11* (19), 11873–11884. https://doi.org/10.1021/acscatal.1c03471.
- (44) Sushkevich, V. L.; Palagin, D.; van Bokhoven, J. A. The Effect of the Active-Site Structure on the Activity of Copper Mordenite in the Aerobic and Anaerobic Conversion of Methane into Methanol. *Angew. Chem. Int. Ed.* **2018**, *57* (29), 8906–8910. https://doi.org/10.1002/anie.201802922.
- (45) Fischer, J. W. A.; Brenig, A.; Klose, D.; Van Bokhoven, J. A.; Sushkevich, V. L.; Jeschke, G. Methane Oxidation over Cu ²⁺ /[CuOH] ⁺ Pairs and Site-Specific Kinetics in Copper Mordenite Revealed by Operando Electron Paramagnetic Resonance and UV/Visible Spectroscopy. *Angew. Chem. Int. Ed.* **2023**, e202303574. https://doi.org/10.1002/anie.202303574.
- (46) Ikuno, T.; Grundner, S.; Jentys, A.; Li, G.; Pidko, E.; Fulton, J.; Sanchez-Sanchez, M.; Lercher, J. A. Formation of Active Cu-Oxo Clusters for Methane Oxidation in Cu-Exchanged Mordenite. *J. Phys. Chem. C* **2019**, *123* (14), 8759–8769. https://doi.org/10.1021/acs.jpcc.8b10293.
- (47) Heyer, A. J.; Plessers, D.; Braun, A.; Rhoda, H. M.; Bols, M. L.; Hedman, B.; Hodgson, K. O.; Schoonheydt, R. A.; Sels, B. F.; Solomon, E. I. Methane Activation by a Mononuclear Copper Active Site in the Zeolite Mordenite: Effect of Metal Nuclearity on Reactivity. *J. Am. Chem. Soc.* **2022**, *144* (42), 19305–19316. https://doi.org/10.1021/jacs.2c06269.
- (48) Mahyuddin, M. H.; Staykov, A.; Shiota, Y.; Miyanishi, M.; Yoshizawa, K. Roles of Zeolite Confinement and Cu–O–Cu Angle on the Direct Conversion of Methane to Methanol by [Cu $_2$ (μ -O)] $^{2+}$ -Exchanged AEI, CHA, AFX, and MFI Zeolites. *ACS Catal.* **2017**, *7* (6), 3741–3751. https://doi.org/10.1021/acscatal.7b00588.
- (49) Mahyuddin, M. H.; Shiota, Y.; Yoshizawa, K. Methane Selective Oxidation to Methanol by Metal-Exchanged Zeolites: A Review of Active Sites and Their Reactivity. *Catal. Sci. Technol.* **2019**, *9* (8), 1744–1768. https://doi.org/10.1039/C8CY02414F.
- (50) Goodman, B. R.; Schneider, W. F.; Hass, K. C.; Adams, J. B. Theoretical Analysis of Oxygen-Bridged Cu Pairs in Cu-Exchanged

- Zeolites. Catal. Lett. **1998**, 56 (4), 183–188. https://doi.org/10.1023/A:1019029700959.
- (51) Goodman, B. R.; Hass, K. C.; Schneider, W. F.; Adams, J. B. Cluster Model Studies of Oxygen-Bridged Cu Pairs in Cu–ZSM-5 Catalysts. *J. Phys. Chem. B* **1999**, *103* (47), 10452–10460. https://doi.org/10.1021/jp9922110.
- (52) Rice, M. J.; Chakraborty, A. K.; Bell, A. T. Theoretical Studies of the Coordination and Stability of Divalent Cations in ZSM-5. *J. Phys. Chem. B* **2000**, *104* (43), 9987–9992. https://doi.org/10.1021/jp0009352.
- (53) Da Costa, P.; Modén, B.; Meitzner, G. D.; Lee, D. K.; Iglesia, E. Spectroscopic and Chemical Characterization of Active and Inactive Cu Species in NO Decomposition Catalysts Based on Cu-ZSM5. *Phys Chem Chem Phys* **2002**, *4* (18), 4590–4601. https://doi.org/10.1039/B203700A.
- (54) Xie, P.; Pu, T.; Aranovich, G.; Guo, J.; Donohue, M.; Kulkarni, A.; Wang, C. Bridging Adsorption Analytics and Catalytic Kinetics for Metal-Exchanged Zeolites. *Nat. Catal.* **2021**, *4* (2), 144–156. https://doi.org/10.1038/s41929-020-00555-0.
- (55) Fickel, D. W.; Lobo, R. F. Copper Coordination in Cu-SSZ-13 and Cu-SSZ-16 Investigated by Variable-Temperature XRD. *J. Phys. Chem. C* **2010**, *114* (3), 1633–1640. https://doi.org/10.1021/jp9105025.
- (56) Kvande, K.; Garetto, B.; Deplano, G.; Signorile, M.; Solemsli, B. G.; Prodinger, S.; Olsbye, U.; Beato, P.; Bordiga, S.; Svelle, S.; Borfecchia, E. Understanding C–H Activation in Light Alkanes over Cu-MOR Zeolites by Coupling Advanced Spectroscopy and Temperature-Programmed Reduction Experiments. *Chem. Sci.* **2023**, *14* (36), 9704–9723. https://doi.org/10.1039/D3SC01677C.
- (57) Martini, A.; Borfecchia, E.; Lomachenko, K. A.; Pankin, I. A.; Negri, C.; Berlier, G.; Beato, P.; Falsig, H.; Bordiga, S.; Lamberti, C. Composition-Driven Cu-Speciation and Reducibility in Cu-CHA Zeolite Catalysts: A Multivariate XAS/FTIR Approach to Complexity. *Chem. Sci.* **2017**, *8* (10), 6836–6851. https://doi.org/10.1039/C7SC02266B.
- (58) Alayon, E. M. C.; Nachtegaal, M.; Bodi, A.; van Bokhoven, J. A. Reaction Conditions of Methane-to-Methanol Conversion Affect the Structure of Active Copper Sites. *ACS Catal.* **2014**, *4* (1), 16–22. https://doi.org/10.1021/cs400713c.
- (59) Kresse, G.; Furthmüller, J. Efficient Iterative Schemes for Ab Initio Total-Energy Calculations Using a Plane-Wave Basis Set. *Phys. Rev. B* **1996**, 54 (16), 11169–11186. https://doi.org/10.1103/PhysRevB.54.11169.
- (60) Blöchl, P. E. Projector Augmented-Wave Method. *Phys. Rev. B* **1994**, *50* (24), 17953–17979. https://doi.org/10.1103/PhysRevB.50.17953.
- (61) Kresse, G.; Joubert, D. From Ultrasoft Pseudopotentials to the Projector Augmented-Wave Method. *Phys. Rev. B* **1999**, *59* (3), 1758–1775. https://doi.org/10.1103/PhysRevB.59.1758.
- (62) Grimme, S.; Antony, J.; Ehrlich, S.; Krieg, H. A Consistent and Accurate *Ab Initio* Parametrization of Density Functional Dispersion Correction (DFT-D) for the 94 Elements H-Pu. *J. Chem. Phys.* **2010**, *132* (15), 154104. https://doi.org/10.1063/1.3382344.
- (63) Grimme, S.; Ehrlich, S.; Goerigk, L. Effect of the Damping Function in Dispersion Corrected Density Functional Theory. *J. Comput. Chem.* **2011**, *32* (7), 1456–1465. https://doi.org/10.1002/jcc.21759.
- (64) Campbell, C. T.; Sellers, J. R. V. The Entropies of Adsorbed Molecules. *J. Am. Chem. Soc.* **2012**, *134* (43), 18109–18115. https://doi.org/10.1021/ja3080117.
- (65) Wang, G.; Zhi, C.; Wang, Y.; Wang, Q. Theoretical Investigation on the Structure-Activity Relationship for Methane Activation in Cu-CHA Zeolite. *Comput. Theor. Chem.* **2023**, 114228. https://doi.org/10.1016/j.comptc.2023.114228.
- (66) Wijerathne, A.; Sawyer, A.; Daya, R.; Paolucci, C. Competition between Mononuclear and Binuclear Copper Sites across Different Zeolite Topologies. *JACS Au* **2024**, *4* (1), 197–215. https://doi.org/10.1021/jacsau.3c00632.
- (67) Sushkevich, V. L.; Smirnov, A. V.; van Bokhoven, J. A. Autoreduction of Copper in Zeolites: Role of Topology, Si/Al Ratio, and Copper Loading. *J. Phys. Chem. C* **2019**, *123* (15), 9926–9934. https://doi.org/10.1021/acs.jpcc.9b00986.
- (68) Sushkevich, V. L.; Safonova, O. V.; Palagin, D.; Newton, M. A.; Van Bokhoven, J. A. Structure of Copper Sites in Zeolites Examined by Fourier and Wavelet Transform Analysis of EXAFS. *Chem. Sci.* **2020**, *11* (20), 5299–5312. https://doi.org/10.1039/D0SC01472A.
- (69) Borfecchia, E.; Pappas, D. K.; Dyballa, M.; Lomachenko, K. A.; Negri, C.; Signorile, M.; Berlier, G. Evolution of Active Sites during Selective Oxidation of Methane to Methanol over Cu-CHA and Cu-MOR Zeolites as Monitored by Operando XAS. *Catal. Today* **2019**, *333*, 17–27. https://doi.org/10.1016/j.cattod.2018.07.028.

- (70) Wieser, J.; Knorpp, A. J.; Stoian, D. C.; Rzepka, P.; Newton, M. A.; Van Bokhoven, J. A. Assessing the Productivity of the Direct Conversion of Methane-to-Methanol over Copper-Exchanged Zeolite Omega (MAZ) via Oxygen Looping. *Angew. Chem. Int. Ed.* **2023**, *62* (40), e202305140. https://doi.org/10.1002/anie.202305140.
- (71) Pidko, E. A.; Hensen, E. J. M.; van Santen, R. A. Self-Organization of Extraframework Cations in Zeolites. *Proc. R. Soc. Math. Phys. Eng. Sci.* **2012**, 468 (2143), 2070–2086. https://doi.org/10.1098/rspa.2012.0057.
- (72) Giordanino, F.; Vennestrøm, P. N. R.; Lundegaard, L. F.; Stappen, F. N.; Mossin, S.; Beato, P.; Bordiga, S.; Lamberti, C. Characterization of Cu-Exchanged SSZ-13: A Comparative FTIR, UV-Vis, and EPR Study with Cu-ZSM-5 and Cu-β with Similar Si/Al and Cu/Al Ratios. *Dalton Trans.* **2013**, *42* (35), 12741. https://doi.org/10.1039/c3dt50732g.
- (73) Smeets, P. J.; Groothaert, M. H.; Schoonheydt, R. A. Cu Based Zeolites: A UV–Vis Study of the Active Site in the Selective Methane Oxidation at Low Temperatures. *Catal. Today* **2005**, *110* (3–4), 303–309. https://doi.org/10.1016/j.cattod.2005.09.028.
- (74) Beznis, N. V.; Weckhuysen, B. M.; Bitter, J. H. Cu-ZSM-5 Zeolites for the Formation of Methanol from Methane and Oxygen: Probing the Active Sites and Spectator Species. *Catal. Lett.* **2010**, *138* (1–2), 14–22. https://doi.org/10.1007/s10562-010-0380-6.
- (75) Vanelderen, P.; Vancauwenbergh, J.; Tsai, M.-L.; Hadt, R. G.; Solomon, E. I.; Schoonheydt, R. A.; Sels, B. F. Spectroscopy and Redox Chemistry of Copper in Mordenite. *ChemPhysChem* **2014**, *15* (1), 91–99. https://doi.org/10.1002/cphc.201300730.
- (76) Larsen, S. C.; Aylor, A.; Bell, A. T.; Reimer, J. A. Electron Paramagnetic Resonance Studies of Copper Ion-Exchanged ZSM-5. *J. Phys. Chem.* **1994**, *98* (44), 11533–11540. https://doi.org/10.1021/j100095a039.
- (77) Iacobone, U.; Nova, I.; Tronconi, E.; Villamaina, R.; Ruggeri, M. P.; Collier, J.; Thompsett, D. Transient CO Oxidation as a Versatile Technique to Investigate Cu2+ Titration, Speciation and Sites Hydrolysis on Cu–CHA Catalysts: The Cu Loading Effect. *Top. Catal.* **2023**, *66* (13–14), 761–770. https://doi.org/10.1007/s11244-023-01813-8.

- (78) Sushkevich, V. L.; van Bokhoven, J. A. Revisiting Copper Reduction in Zeolites: The Impact of Autoreduction and Sample Synthesis Procedure. *Chem. Commun.* **2018**, *54* (54), 7447–7450. https://doi.org/10.1039/C8CC03921F.
- (79) Engedahl, U.; Boje, A.; Ström, H.; Grönbeck, H.; Hellman, A. Complete Reaction Cycle for Methane-to-Methanol Conversion over Cu-SSZ-13: First-Principles Calculations and Microkinetic Modeling. *J. Phys. Chem. C* **2021**, *125* (27), 14681–14688. https://doi.org/10.1021/acs.jpcc.1c04062.
- (80) Occhiuzzi, M.; Fierro, G.; Ferraris, G.; Moretti, G. Unusual Complete Reduction of Cu ²⁺ Species in Cu-ZSM-5 Zeolites under Vacuum Treatment at High Temperature. *Chem. Mater.* **2012**, *24* (11), 2022–2031. https://doi.org/10.1021/cm203796u.
- (81) Newton, M. A.; Knorpp, A. J.; Pinar, A. B.; Sushkevich, V. L.; Palagin, D.; Van Bokhoven, J. A. On the Mechanism Underlying the Direct Conversion of Methane to Methanol by Copper Hosted in Zeolites; Braiding Cu K-Edge XANES and Reactivity Studies. *J. Am. Chem. Soc.* **2018**, *140* (32), 10090–10093. https://doi.org/10.1021/jacs.8b05139.
- (82) Dyballa, M.; Thorshaug, K.; Pappas, D. K.; Borfecchia, E.; Kvande, K.; Bordiga, S.; Berlier, G.; Lazzarini, A.; Olsbye, U.; Beato, P.; Svelle, S.; Arstad, B. Zeolite Surface Methoxy Groups as Key Intermediates in the Stepwise Conversion of Methane to Methanol. *ChemCatChem* **2019**, *11* (20), 5022–5026. https://doi.org/10.1002/cctc.201901315.
- (83) Sushkevich, V. L.; Verel, R.; Bokhoven, J. A. Pathways of Methane Transformation over Copper-Exchanged Mordenite as Revealed by In Situ NMR and IR Spectroscopy. *Angew. Chem. Int. Ed.* **2020**, *59* (2), 910–918. https://doi.org/10.1002/anie.201912668.
- (84) Wu, J.-F.; Gao, X.-D.; Wu, L.-M.; Wang, W. D.; Yu, S.-M.; Bai, S. Mechanistic Insights on the Direct Conversion of Methane into Methanol over Cu/Na–ZSM-5 Zeolite: Evidence from EPR and Solid-State NMR. *ACS Catal.* **2019**, 9 (9), 8677–8681. https://doi.org/10.1021/acscatal.9b02898.

